

**ASYMPTOTIC BEHAVIOUR OF GRAVITY  
DRIVEN FREE SURFACE FLOWS  
RESULTING FROM CAVITY COLLAPSE**

**A Thesis Submitted to  
the Graduate School of Engineering and Sciences of  
İzmir Institute of Technology  
in Partial Fulfillment of the Requirements for the Degree of**

**DOCTOR OF PHILOSOPHY**

**in Mathematics**

**by  
Elona FETAHU**

**July 2020  
İZMİR**

To my parents  
Nazire and Yzeir

## ACKNOWLEDGMENTS

I would like to express my gratitude to my advisor, Prof. Dr. Oğuz YILMAZ, who expertly guided me during my Ph.D. studies. He worked tirelessly and patiently to help me develop a better understanding on the subject. I want to thank him for his enthusiasm on the topic and his support, that kept me motivated about my research. I feel glad and privileged to have worked with him.

It is a pleasure to thank Prof. Dr. Aleksander. A. KOROBKIN, who suggested the problems treated in this thesis, and assisted with his insightful comments.

My appreciation extends to Assoc. Prof. Dr. Olha IVANYSHYN YAMAN, for being so willing to help with the solution of the integral equation in the third problem of this thesis.

To the jury members that followed my thesis progress, Prof. Dr. Oktay PASHAEV and Prof. Dr. Nejat BULUT, I am grateful for the ideas and the suggestions they shared during the presentations.

My stay in Turkey during my Ph.D. studies was financed by Turkish Scholarships, to which I greatly acknowledge.

I owe my gratitude to my friends at Izmir Institute of Technology, for their unconditional support and for making my stay in Turkey so joyful and feel like at home.

I would like to say a heartfelt thank you to my family for motivating me and being always by my side. I want to thank my biggest blessing, mom and dad, for being the best examples to follow in life and for never stopping believing in me.

# ABSTRACT

## ASYMPTOTIC BEHAVIOUR OF GRAVITY DRIVEN FREE SURFACE FLOWS RESULTING FROM CAVITY COLLAPSE

In this thesis, the gravity driven potential flows that result from cavity collapse are studied. Initially, the collapse of a vertical cylindrical cavity of circular cross sections surrounded by a liquid region is examined for two different situations. In the first one the cavity has same depth as the fluid and in the second one the cavity starts from the free surface and has less depth than the fluid. The problem is formulated by using a small parameter that represents the short duration of the stage. The first problem, as the radius and the centre of the cavity approach infinity, reduces to the classical two-dimensional dam break problem solved by Korobkin and Yilmaz (2009). The singularity of the radial velocity at the bottom circle is shown to be of logarithmic type. In the second problem, where the cavity is less deep than the fluid, the flow region is separated into two regions: the interior one, which is underneath the cylindrical cavity and above the rigid bottom, and the exterior one, which is the rest of the flow. The corresponding new problems are solved separately and then the coefficients are found by applying the matching conditions at the interface, where the fluid radial velocities and pressures coincide. On the limiting case, the problem reduces to the two-dimensional dam break flow of two immiscible fluids by Yilmaz et al. (2013a). Singularity at the bottom circle of the cavity is observed, which is of the same type as in the latter paper. Next, a third problem studies the gravity driven flow caused by the collapse of a rectangular section of a vertical plate. During the early stage, the flow is described by the velocity potential. Attention is paid to determining the velocity potential and free surface shapes. The solution follows the Fourier series method in Renzi and Dias (2013) and the boundary element method in Yilmaz et al. (2013a). Singularity is observed at the side edges and lower edge of the rectangular section. The horizontal velocity of the initially vertical free surface along the vertical line of symmetry of the rectangle is the same to the one in the two-dimensional problem Korobkin and Yilmaz (2009). The singularities observed in these problems lead to the jet formation for the initial stage. The methods applied in these computations are expected to be helpful in the analysis of gravity-driven flow free surface shapes. This thesis is a contribution towards the 3-D generalizations of dam break problems.

## ÖZET

### KAVİTASYON ÇÖKMESİYLE OLUŞAN, YERÇEKİMİ ETKİSİNDEKİ SERBEST YÜZEYLİ AKIŞLARIN ASİMTOTİK DAVRANIŞI

Bu tezde, kavitasyon çökmesi sonucu oluşan yer çekimine dayalı potansiyel akışlar incelenecektir. Başlangıçta, bir sıvı bölge ile çevrili ara kesiti dairesel olan bir dik silindirin kavitasyon çökmesi iki farklı durum için incelenir. İlk durumda, kavitasyon sıvı ile aynı derinliğe sahiptir ve ikinci durumda, kavitasyon serbest yüzeyden başlar ve sıvıdan daha az derinliğe sahiptir. Problem, kademelerin kısa süresini temsil eden küçük bir parametre kullanılarak formüle edilir. Birinci problemde, kavitasyonun merkezi ile yarıçapı sonsuzluğa yaklaştığında, problemin Korobkin and Yılmaz (2009) tarafından çözülen klasik iki boyutlu baraj kırılma problemine dönüştüğünü göstereceğiz. Alttaki daire içindeki radyal hızın tekillik analizi logaritmik tipte olması bekleniyor. İkinci problemde, kavitasyonun sıvıdan daha az derin olduğu yerde, akış bölgesi silindirik kavitasyonun altındaki iç bölge ve akışın geri kalanı olan dış bölge olmak üzere iki bölgeye ayrılır. İlgili yeni problemler ayrı ayrı çözülür ve daha sonra katsayılar, akışkan radyal hızlarının ve basınçlarının aynı olduğu arayüzde eşleştirilerek bulunur. Yarıçapın ve kavitasyonun merkezinin sonsuzluğa yaklaştığı sınırlayıcı durumda, problem Yılmaz et al. (2013a) tarafından iki karışmaz sıvının iki boyutlu baraj kırılma akışına indirgenir. Kavitasyonun alt dairesinde, ikinci çalışmadaki aynı tip, tekillik gözlenir. Daha sonra, üçüncü bir problemde, dikey bir plakanın dikdörtgen bir bölümünün çökmesinden kaynaklanan yer çekimine dayalı akışı incelenir. Erken aşamada, akış hız potansiyeli ile tanımlanır. Hız potansiyelinin ve serbest yüzey şekillerinin belirlenmesine dikkat edilir. Çözüm, Renzi and Dias (2013)'deki Fourier serisi yöntemini ve Yılmaz et al. (2013a)'daki sınır elemanı yöntemini izler. Dikdörtgensel kesitin yan ve alt kenarlarında tekillik gözlenir. Başlangıçta dikey serbest yüzeyin yatay hızı, dikdörtgenin dikey simetri çizgisi boyunca iki boyutlu problem Korobkin and Yılmaz (2009) ile aynıdır. Bu problemlerde gözlenen tekillikler, ilk aşama için jet oluşumuna yol açar. Bu hesaplamalarda kullanılan yöntemlerin, yerçekimine dayalı serbest yüzey şekillerinin analizinde yararlı olması beklenmektedir. Bu tez, baraj kırılma problemlerinin 3-D genellemelerine bir katkıdır.

# TABLE OF CONTENTS

LIST OF FIGURES .....	viii
LIST OF TABLES .....	x
CHAPTER 1. INTRODUCTION .....	1
CHAPTER 2. THE COLLAPSE OF A VERTICAL CYLINDRICAL CAVITY OF CIRCULAR CROSS SECTIONS EXTENDING FROM THE FREE SUR- FACE TO THE BOTTOM OF A SURROUNDING FLUID OF FINITE DEPTH	7
2.1. Formulation of the problem .....	7
2.2. Leading-order outer problem and solution by the Fourier series method .....	11
2.3. Reduction to the 2-D problem .....	13
2.4. Analysis of the singularity of the radial velocity at the bottom circle	13
2.5. Numerical results .....	15
2.5.1. Velocities of the free surfaces.....	15
2.5.2. Free surface shapes.....	17
CHAPTER 3. THE COLLAPSE OF A VERTICAL CYLINDRICAL CAVITY OF CIRCULAR CROSS SECTIONS EXTENDING FROM THE FREE SUR- FACE AND HAVING LESS DEPTH THAN A SURROUNDING FLUID OF FINITE DEPTH .....	20
3.1. Formulation of the problem .....	21
3.1.1. Leading-order outer problem .....	24
3.2. Solution by the Fourier series method .....	27
3.3. Reduction to the 2-D problem .....	29
3.4. Singularity analysis near the bottom circle.....	30
3.5. Nonlinear analysis at the bottom circle.....	32
3.6. Numerical results .....	33
3.6.1. Convergence of the coefficients.....	34

3.6.2. Radial and vertical velocities along the interface .....	34
3.6.3. Velocities of the free surfaces.....	36
3.6.4. Free surface shapes.....	38
CHAPTER 4. THE GRAVITY DRIVEN FREE SURFACE FLOW CAUSED BY THE COLLAPSE OF A RECTANGULAR SECTION OF A VERTICAL PLATE	
43	
4.1. Formulation of the problem .....	44
4.2. Leading-order outer problem and solution by boundary element method .....	47
4.2.1. First problem: The Green's function is zero at $x = 0$ .....	52
4.2.2. Second problem: The derivative of the Green's function is zero at $x = 0$ .....	59
4.3. Numerical results .....	63
CHAPTER 5. CONCLUSIONS .....	68
REFERENCES .....	71
APPENDICES	
APPENDIX A. MODIFIED BESSEL FUNCTIONS $I$ AND $K$ .....	74
A.1. Definition and properties .....	74
A.2. Asymptotic expansions for large arguments .....	74
A.3. Limiting forms for small arguments .....	75
A.4. Differentiation with respect to $w$ .....	75
APPENDIX B. DIRAC DELTA FUNCTION .....	76
APPENDIX C. GREEN'S FUNCTION FOR THE HELMHOLTZ EQUATION ....	77

# LIST OF FIGURES

<u>Figure</u>	<u>Page</u>
Figure 1.1. Flow region at $t = 0$ for the 2-D problem by Korobkin and Yilmaz (2009) .....	4
Figure 1.2. Gravity-driven flow for two immiscible fluids a) at rest, b) at the instant when the plate collapses, c) after the collapse by Yilmaz et al. (2013a) ..	5
Figure 2.1. Flow region at initial time $t' = 0$ .....	8
Figure 2.2. Radial velocity $\varphi_{0,r}(a/H, z, t)$ of the initially vertical free surface for $a/H = 0.5, 1, 2$ . .....	16
Figure 2.3. Radial velocity $\varphi_{0,r}(r, -1, t)$ along the rigid bottom for $a/H = 0.5, 1, 2$ . .	17
Figure 2.4. Top free surface at time $t = 1$ , $\varepsilon = 0.01$ , $a/H = 0.5$ , $a/H = 1$ , $a/H = 2$ and 2D .....	19
Figure 2.5. Vertical free surface at time $t = 1$ , $\varepsilon = 0.01$ , $a/H = 0.5$ , $a/H = 1$ , $a/H = 2$ and 2D .....	19
Figure 3.1. Flow region at initial time $t' = 0$ .....	21
Figure 3.2. Shift from $xyz$ to $\tilde{x}\tilde{y}\tilde{z}$ coordinate system .....	31
Figure 3.3. Boundary value problem describing the local flow near the bottom circle. ....	32
Figure 3.4. Radial velocities $\phi_r^\pm(a/H^+, z)$ of the interface for $\delta = 0.5$ . ....	35
Figure 3.5. Vertical velocities $\phi_z^\pm$ of the interface for $\delta = 0.5$ . ....	36
Figure 3.6. Radial velocity of the initially vertical free surface $\varphi_{0,r}^+(a/H^+, z, t)$ for $a/H^+ = 0.5, 1, 1.5$ . and 2-D .....	37
Figure 3.7. Vertical velocity of the lower free surface $\varphi_{0,z}^-(r, \delta, t)$ for $a/H^+ = 0.5, 1, 1.5$ . and 2-D .....	38
Figure 3.8. Top free surface shape of the 2-D and 3-D case for different ratios $a/H^+ = 0.5, 1, 1.5$ and for $\delta = 0.5$ , $\varepsilon = 0.01$ .....	40
Figure 3.9. Vertical free surface shape for $\delta = 0.5$ and $\varepsilon = 0.01$ computed for the 2-D case and for the 3-D case for different ratios $a/H^+ = 0.5, 1, 1.5$ .....	41
Figure 3.10. Lower free surface shape $v_0$ for $\delta = 0.5$ and $\varepsilon = 0.01$ computed for the 2-D case and for the 3-D case for different ratios $a/H^+ = 0.5, 1, 1.5$ .....	42
Figure 4.1. Flow region at initial time $t' = 0$ .....	43



Figure 4.2. BVP for $\varphi_{0n}$ .....	49
Figure 4.3. The element $j$ does not coincide with element $i$ . .....	55
Figure 4.4. The element $j$ coincides with element $i$ , $a_j = (0, y_j)$ . .....	55
Figure 4.5. Discretization of the rectangular section .....	63
Figure 4.6. Horizontal velocities for $z = -1, -0.9, -0.5, -0.1, 0$ .....	65
Figure 4.7. Horizontal velocities for $y = \pm 0.499, \pm 0.498, \pm 0.4, \pm 0.3, 0$ .....	66
Figure 4.8. 3-D view of the vertical free surface at time $t = 1$ , $\epsilon = 0.01$ , where on the vertical lines $y = \pm 0.499, \pm 0.498, \pm 0.4, \pm 0.3, \pm 0.2, \pm 0.1, 0$ , $z \in S$ , and on the horizontal lines $y \in Q$ , $z = -1, -0.9, -0.8, -0.7, -0.6, -0.5,$ $-0.4, -0.3, -0.2, -0.1, 0$ .....	66
Figure 4.9. Vertical free surface at time $t = 1$ , $\epsilon = 0.01$ for 3-D at $y=0$ compared to 2-D .....	67

# LIST OF TABLES

<u>Table</u>		<u>Page</u>
Table 2.1.	Radial velocity of the initially vertical free surface .....	16
Table 2.2.	Radial velocity along the rigid bottom .....	18
Table 3.1.	Convergence of $d_m$ .....	34
Table 3.2.	Convergence of $c_n$ .....	34
Table 3.3.	Radial velocities along the interface .....	35
Table 3.4.	Vertical velocities along the interface .....	36
Table 3.5.	Radial velocities of the initially vertical free surface near the bottom circle .....	37
Table 3.6.	Vertical velocities of the lower free surface near the bottom circle .....	39

# CHAPTER 1

## INTRODUCTION

Some interesting hydrodynamical problems are the gravity-driven flows caused by cavity collapse. As examples of such motion we can mention the flow towards the cavity of a liquid surrounding a cylindrical cavity. These types of cavities are the idealized form of the cavities formed when we have, for example, explosion at the water surface (see Benusiglio et al. (2014)). Immediately after the explosion, a cavity is created, which, under the gravitational force, is filled with the surrounding liquid. Other examples we can mention are cavity formation by the water entry of projectiles (Truscott et al. (2014)), or air cavity produced by the run on water of some creatures like shore birds and green basilisk lizards (Glasheen and McMahon (1996a), Glasheen and McMahon (1996b)).

Another important problem is the bursting of a dam wall. The investigation of dam-break problems is essential in designing dams and their surroundings. When a dam breaks, the gravitational potential energy of the accumulated water may put in risk everything nearby. Dam-break flow may result in serious consequences for the environment, human lives and property (Singh (1996)). For this reason, these types of problems need to be studied by mathematical models and experiments.

In the Ph.D. thesis of Pohle (1950), the solution of the gravity-driven flow caused by the collapse of a half-cylinder of fluid is solved using Lagrangian representation, where the displacement of each particle is determined following each individual particle while it moves through space and time. The displacements and pressure are thought in time power series. Following same method, Stoker (1957) solved the problem for the dam-breaking and discovered the vertical free surface to be negative infinite at the meeting point of the vertical free surface with the bottom (see Fig. 1.1). Furthermore, he discovers that at the point of contact, the horizontal component of the velocity is logarithmic singular. This shows that the solution is not valid near this point, therefore this solution is considered as an outer solution and an inner solution is needed at a vicinity of the contact point. Korobkin and Pukhnachov (1988) state that the water entry of a blunt object with no flattening at initial stage can be better described by Lagrangian coordinates. So, the Lagrangian

representation is suitable to be used in the cases when there are no intersections of free surfaces with rigid ones. Therefore, concerning the dam-break problems, where these intersections are present, the Lagrangian representation is not very appropriate, and Eulerian representation is used. William George Penney and Thornhill (1952) also worked on the collapse of column of fluid of hemi-cylindrical and hemispherical shape surrounded by a less denser liquid. The problem is solved using Eulerian representation. They show that the initial asymptotics of the solution is not valid at the intersection with the bottom. The inner solution near the contact points was not treated in these studies.

The interesting part of the dam-break problems is the investigation at the points where the free surfaces meet the rigid surfaces, where jet formations are observed in experiments. Among experiments done on dam-break flows, there is the study of Stansby et al. (1998), who undertake some experiments on dam-break flows where a thin vertical sheet separates two liquids of different heights or one side of the sheet is dry and a liquid is resting on the other side. After the release, on the initial stages, they notice a mushroom-like jet for the wet-bed at the line of intersection between the initially vertical surface and the free surface of the shallower liquid. It is observed a horizontal jet at the line where the free surface and the rigid bottom intersect for the dry-bed case. The dam break waves along a smooth horizontal channel for dry bed analytically and experimentally are studied by Lauber and Hager (1998). Janosi et al. (2004) during their experiments on the drag reduction effect notice the formation of a mushroom-like object when the dam between water at a higher depth and shallower coloured water is released.

The presence of a jet is also observed by C. King and Needham (1994) when a vertical plate with an angle  $\alpha = \pi/2$  with the rigid bottom moves uniformly forward into a fluid. As the plate approaches the fluid, which has a free surface, a rise in the free surface is noticed at the intersection of the free surface and plate for the initial stages. To study this jet formation, they perform an asymptotic analysis. At the intersection, singularity is observed in the leading order outer solution, therefore specific attention is paid to the inner region at the point where the jet occurs. The generalization of this problem is the uniformly accelerating inclined plate with the horizontal bottom with  $\alpha = (0, \pi/2) \cup (\pi/2, \pi)$ , studied by Needham et al. (2008). Solution of inner region at the contact point, indicates a weak jet formation for angles  $\alpha = (0, \pi/2)$  and a stronger jet when  $\alpha = (\pi/2, \pi)$ .

Jet formations are also present in the water impact problems at the initial stage. A body's impact onto a liquid's free surface is studied by Korobkin and Pukhnachov (1988), where the body has a plane front section. In that paper it is claimed that the singularity of the velocity field is  $r^{-1/2}$  at the vicinity of the contact point, where  $r$  is the distance from the contact point. Iafrati and Korobkin (2004) study the initial stage of the impact of a flat plate with a liquid's free surface. At the plate edges, they discover singularity in the liquid's velocity for the leading order outer problem. Calculations of the inner solution reveal jet formation at the edges and square root singularity of the flow velocity.

In this thesis we treat two cavity collapse problems and one dam-break problem. The liquids taken in consideration are considered incompressible and inviscid. The liquids are initially at rest. Due to gravity, soon after the collapse, the flow starts. It is three dimensional and irrotational. The problems are studied for the initial stages and are described by the linear potential theory. We employ the Eulerian representation throughout this thesis. In the first problem, the collapse of a cylindrical cavity and the resulting gravity-driven flow are considered. A liquid surrounds the cavity and initially the cylinder is placed at a rigid bottom and extends from the free surface to the base of the surrounding liquid, which is at rest. The cylinder's height is denoted by  $H$  and its radius by  $a$ .

The first cavity collapse problem treated in this thesis to the best of our knowledge has not been studied before. It can be considered as a three dimensional dam-break flow. When the radius is large compared to the liquid depth, this problem reduces to the two dimensional dry-bed dam-break problem. A closely relevant study to this problem is the one by Korobkin and Yilmaz (2009), the initial stage of the classical two dimensional dam-break problem. In that paper the gravity driven flow caused by the collapse of a dam located in front of a liquid region is studied for short times (see Fig. 1.1). The flow is two-dimensional and potential. Attention is paid to the liquid flow and the free surface shapes. Fourier series method and complex analysis is used in solving the leading order and second order outer problems. Near the corner point, the horizontal velocity of the vertical free surface, is found to be log-singular. Furthermore, the analysis of the inner region at the corner point, describes the formation of a jet there.

Similarly, we pose the problem using a parameter as in Korobkin and Yilmaz (2009) to present the small span of the stage. Fourier series method is used to solve the linearised BVP. The velocity field is found to be singular at the bottom circle. The analysis

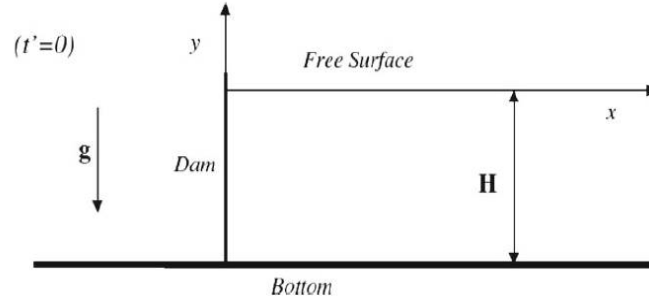


Figure 1.1. Flow region at  $t = 0$  for the 2-D problem by Korobkin and Yilmaz (2009)

of the reduction to the 2-D problem provides the type of the singularity and shows that for big values  $a/H$  the problem becomes quite similar to the classical 2-D dam-break problem. The inner region analysis, that shows the presence of a jet at the bottom circle is omitted, as it will be the same to the 2-D problem.

In the second problem of this thesis, we treat the gravity-driven flow as a result of the collapse of a cylindrical cavity. The cavity is surrounded by a liquid which has a finite depth. The difference with the first problem is that, in this case the cylindrical cavity starts from the free surface, to a distance  $H^-$  from the rigid bottom, that is, the cavity is shorter than the liquid depth. The cylinder is placed at a height  $H^-$  from the base and the liquid depth is  $H^+$ . The radius of the cylinder is  $a$ .

The second cavity collapse problem we treat in this thesis to the best of our knowledge has not been studied before. If the radius  $a$  is big compared to the liquid depth  $H^+$ , this problem can be considered as the two dimensional wet-bed dam-break problem. A strongly related study to this one, is the flow as a result of collapse of a flat sheet separating two immiscible fluids by Yilmaz et al. (2013a). In that paper the flow of two immiscible fluids as a result of gravity is studied. At  $t = 0$ , the fluids are at rest. There is a flat sheet separating them. The fluids have different depths, the one on the right  $H^+$  and the one on the left  $H^-$ , here  $H^- < H^+$  (see Fig. 1.2). When the vertical plate suddenly disappears, the gravity driven flow starts. The problem is studied in its initial stage by the linear potential theory. The flow region is separated into two regions, the liquid on the right and the liquid on the left, and then the pressure conditions and radial velocities are matched at the interface. Boundary element and Fourier series method are used to solve the problem. It is discovered that at the triple point, which is the intersection between the

vertical surface and the shallower liquid's free surface, the velocity field is power singular  $r^{-\alpha}$ . At the corner point, which is the meeting point between the rigid bottom and interface, it is logarithmic singular. Depending on the density, the power of the singularity varies. The lighter is the deeper liquid, the more singular is the flow. In the case where the density ratio of two liquids is the same, at the triple point, the singularity is  $r^{-1/3}$ , and the singularity at the bottom corner point disappears. A jet-like flow is observed at the triple point by Yilmaz et al. (2013b).

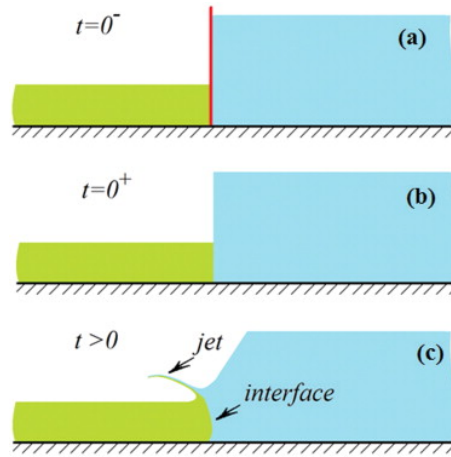


Figure 1.2. Gravity-driven flow for two immiscible fluids a) at rest, b) at the instant when the plate collapses, c) after the collapse by Yilmaz et al. (2013a)

In the second problem of this thesis, similar method will be used, that is we will separate the flow region in two, the interior one, which is the one below the bottom circle of the cylindrical cavity extending to the rigid bottom, and the exterior region, which is rest of the region. Fourier series method will be used to solve the leading order problems separately in both regions, and then they will be matched at the interface, where the pressures of the fluids are equal and the radial velocities too. Attention will be paid to the bottom circle of the cavity, where the jet formation is expected. Analysis at the bottom circle of the cavity shows the type of singularity.

In the third problem, we study the collapse of a rectangular section (dam) of an infinite plate. On one side of the plate the liquid is located, and the other side is dry. The plate is positioned along the  $y'$ -axis, and the liquid is placed on the positive  $x'$ -axis side extending to infinity in the radial direction. The solution is represented in  $(x', y', z')$ , the Cartesian coordinates, where the prime denotes the dimensional variables. The centre of the coordinates is placed at the top line of the plate, where the  $y'$  axis lies. The plate's

height is  $H$  and its length extends to infinity along the  $y$ -axis. The rectangular section is located at  $x' = 0$ ,  $-b \leq y' \leq b$ ,  $-H < z' \leq 0$ .

Renzi and Dias (2012) and Renzi and Dias (2013) derive a potential flow model for an oscillating wave energy in a straight channel and in the open ocean respectively. The problems are solved within the linear potential theory. The BVP is solved using the Green's theorem and then integral-equation technique is applied. In the solution Chebyshev polynomials are used.

The solution method of the third problem will follow Renzi and Dias (2012) and Renzi and Dias (2013) to solve a modified Helmholtz equation. Further, we employ the Green's function (see Linton (1998)) to solve the BVP. This involves the formulation of integral equations, whose kernel is a Green's function, whose solutions are found numerically by using BEM (see Yilmaz et al. (2013a) and Fenner (2014)). The velocities of the initially vertical free surface are plotted along the horizontal and vertical lines on the rectangular gate in order to observe the singularities near the side edges and bottom edge of the rectangular section. To determine the types of singularities, the results from the 2-D dam break problem (Korobkin and Yilmaz (2009) and Yilmaz et al. (2013a)) and the results from the water impact problems (Korobkin and Pukhnachov (1988) and Iafrati and Korobkin (2004)) are used.

The structure of the thesis is as follows:

Chapter 2 formulates and solves by Fourier series method the initial stage of cylindrical cavity collapse flow, where the cylinder and the surrounding liquid have equal depths, which is a 3-D generalization of the classical 2-D problem.

The formulation and solution by Fourier series method for the initial stage of a flow caused by cylindrical cavity collapse, where the cavity is surrounded by a deeper liquid, is provided in Chapter 3. This is a 3-D generalization of the 2-D problem of two immiscible fluids.

Chapter 4 formulates and uses boundary element method to solve the gravity driven flow as a result of the collapse of a rectangular section of a vertical plate.

Finally the conclusions are shown in Chapter 5.



## CHAPTER 2

# THE COLLAPSE OF A VERTICAL CYLINDRICAL CAVITY OF CIRCULAR CROSS SECTIONS EXTENDING FROM THE FREE SURFACE TO THE BOTTOM OF A SURROUNDING FLUID OF FINITE DEPTH

Three dimensional unsteady problem of gravity-driven flow caused by the collapse of a cylindrical cavity surrounded by a liquid region of finite depth is studied. The liquid has the same height as the cylinder and is considered to be inviscid and incompressible. Initially, when the liquid is at rest, the fluid region lies outside the cylindrical cavity and extends to infinity in the radial direction:  $r' > a$ ,  $0 \leq \theta < 2\pi$ ,  $-H < z' \leq 0$ . Here  $r'$ ,  $\theta$ ,  $z'$  represent the circular cylindrical coordinates,  $a$  is the radius of the cylinder,  $H$  is the liquid depth, and the prime stands for the dimensional variables (see Fig.2.1).

At time  $t' = 0$ , the liquid region is bounded by: the top free surface  $r' > a$ ,  $0 \leq \theta < 2\pi$ ,  $z' = 0$ , the vertical free surface  $r' = a$ ,  $0 \leq \theta < 2\pi$ ,  $-H < z' < 0$ , and the rigid bottom  $z' = -H$ , which is dry for  $r' < a$ ,  $0 \leq \theta < 2\pi$ .

With the instant removal of the cylinder, the fluid motion starts flowing towards the cavity. The fluid motion is considered irrotational and the flow is potential. Attention is paid to determining the resulting flow and the free surface shapes at the early stage of the process.

A relevant study is the initial stage of the limiting case, studied by Korobkin and Yilmaz (2009) for the two dimensional gravity driven flow caused by the collapse of a vertical dam located in front of a liquid region. In that paper Fourier series method and complex analysis are used in solving the leading order and second order outer problems and determining the liquid flow and free surface shapes. The analysis at the bottom point, revealed that the horizontal velocity of the initially vertical free surface is log-singular there. In this chapter, similarly we use Fourier series method to solve the 3-D problem and compare the results with the 2-D problem.

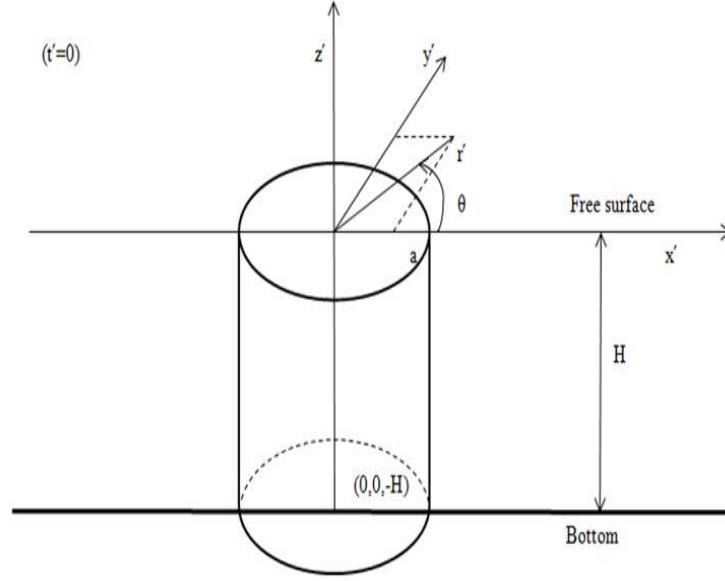


Figure 2.1. Flow region at initial time  $t' = 0$

## 2.1. Formulation of the problem

The fluid motion is considered to be irrotational, implying the existence of a velocity potential  $\varphi'(r', \theta, z', t')$ . Assuming the fluid is incompressible, the dimensional velocity potential  $\varphi'$  satisfies the Laplace's equation

$$\nabla^2 \varphi' = 0 \quad (\text{in } \Omega'(t')), \quad (2.1)$$

where  $\Omega'(t')$  is the flow region bounded by the free surface  $FS'(t')$ , which consists of the horizontal free surface  $TS'$  and the vertical free surface  $VS'$ , and the rigid bottom  $BS'(t')$ . At  $t'=0$ , the cavity starts collapsing (the liquid starts filling the cylindrical cavity) with some deformation of the free surface. We denote the top free surface by  $TS'(t')$ :  $r' > a$ ,  $0 \leq \theta < 2\pi$ ,  $z' = \eta'(r', \theta, t')$  and the vertical free surface by  $VS'(t')$ :  $r' = a + h'(z', \theta, t')$ ,  $0 \leq \theta < 2\pi$ ,  $-H < z' < \eta'(a, \theta, t')$ . It is of interest finding the free surfaces  $z' = \eta'(r', \theta, t')$  and  $r' = a + h'(z', \theta, t')$ . For this purpose, the conditions on these free surfaces should be applied. The kinematic condition on the free surface requires that the fluid particles on

the free surface remain on the free surface,

$$\varphi'_{z'} = \varphi'_{r'} \eta'_{r'} + \frac{1}{r'^2} \varphi'_{\theta} \eta'_{\theta} + \eta'_{r'} \quad (\text{on } TS'(t')), \quad (2.2)$$

$$\varphi'_{r'} = \varphi'_{z'} h'_{z'} + \frac{1}{r'^2} \varphi'_{\theta} h'_{\theta} + h'_{r'} \quad (\text{on } VS'(t')). \quad (2.3)$$

Bernoulli's equation for unsteady irrotational flow is

$$-\frac{p'}{\rho_0} = \varphi'_{t'} + \frac{1}{2} |\nabla \varphi'|^2 + gz' \quad (\text{in } \Omega'(t')). \quad (2.4)$$

By virtue of the fluid being inviscid, the dynamic condition at the free surface, is that the pressure is equal to the atmospheric pressure  $p_0$ ,

$$\varphi'_{t'} + \frac{1}{2} |\nabla \varphi'|^2 + gz' = 0 \quad (\text{on } FS'(t')). \quad (2.5)$$

The bottom is rigid at  $z' = -H$ , meaning that there is no vertical velocity component on this surface

$$\varphi'_{z'} = 0 \quad (\text{on } BS'(t')). \quad (2.6)$$

Initially at  $t' = 0$  there is no flow, and the free surfaces are at their initial positions

$$\varphi'(r', \theta, z', 0) = 0, \quad \eta'(r', \theta, 0) = 0, \quad h'(z', \theta, 0) = 0. \quad (2.7)$$

The fluid is at rest at the far field

$$\varphi' \rightarrow 0 \quad (r' \rightarrow +\infty). \quad (2.8)$$

We introduce the non-dimensional variables in order to reformulate the problem in dimensionless equations

$$\begin{aligned}
r' &= rH, & z' &= zH, & t' &= Tt, \\
\varphi' &= gHT\varphi, & p' &= \rho_0gHp, & T &= \varepsilon^{1/2} \sqrt{H/g}, \\
\eta' &= S_1\eta, & h' &= S_2h, \\
S_1/H &= O(\varepsilon), & S_2/H &= O(\varepsilon).
\end{aligned}$$

The non-dimensional form of the bvp (2.1)-(2.8) is expressed by the following equations

$$\nabla^2\varphi = 0 \quad (\text{in } \Omega(t)), \quad (2.9)$$

$$\varphi_z = \varepsilon\varphi_r\eta_r + \frac{\varepsilon}{r^2}\varphi_\theta\eta_\theta + \eta_t \quad (\text{on } TS(t)), \quad (2.10)$$

$$\varphi_r = \varepsilon\varphi_z h_z + \frac{\varepsilon}{r^2}\varphi_\theta h_\theta + h_t \quad (\text{on } VS(t)), \quad (2.11)$$

$$-p = \varphi_t + \frac{1}{2}\varepsilon|\nabla\varphi|^2 + z \quad (\text{in } \Omega(t)), \quad (2.12)$$

$$p = p_0 = \varphi_t + \frac{1}{2}\varepsilon|\nabla\varphi|^2 + z = 0 \quad (\text{on } FS(t)), \quad (2.13)$$

$$\varphi_z = 0 \quad (\text{on } BS(t)), \quad (2.14)$$

$$\varphi(r, \theta, z, 0, \varepsilon) = 0, \quad \eta(r, \theta, 0, \varepsilon) = 0, \quad h(z, \theta, 0, \varepsilon) = 0, \quad (t = 0) \quad (2.15)$$

$$\varphi \rightarrow 0 \quad (r \rightarrow +\infty). \quad (2.16)$$

Here  $\Omega(t)$  is the flow region bounded by the free surface and the rigid bottom.  $FS(t)$  is the free surface of the region, composed by the top free surface  $TS(t)$ :  $r > a/H$ ,  $0 \leq \theta < 2\pi$ ,  $z = \varepsilon\eta(r, \theta, t, \varepsilon)$ , and the vertical free surface  $VS(t)$ :  $r = a/H + \varepsilon h(z, \theta, t, \varepsilon)$ ,  $0 \leq \theta < 2\pi$ ,  $-1 < z < \varepsilon\eta(a/H, \theta, t, \varepsilon)$ .  $BS(t)$  is the bottom surface  $z = -1$ .

In order to linearise the problem, we search for a solution of (2.9)-(2.16), as  $\varepsilon \rightarrow 0$  in the form

$$\begin{aligned}
\varphi(r, \theta, z, t, \varepsilon) &= \varphi_0(r, \theta, z, t) + \varepsilon\varphi_1(r, \theta, z, t) + O(\varepsilon^2), \\
\eta(r, \theta, t, \varepsilon) &= \eta_0(r, \theta, t) + \varepsilon\eta_1(r, \theta, t) + O(\varepsilon^2), \\
h(z, \theta, t, \varepsilon) &= h_0(z, \theta, t) + \varepsilon h_1(z, \theta, t) + O(\varepsilon^2).
\end{aligned} \quad (2.17)$$

## 2.2. Leading-order outer problem and solution by the Fourier series method

Substituting the asymptotic expansions (2.17) in (2.9)-(2.16), as  $\varepsilon \rightarrow 0$  we get the boundary-value problem for the leading-order velocity potential. The Laplace's equation (2.9) becomes

$$\nabla^2 \varphi_0 = 0 \quad (r > a/H, 0 \leq \theta < \pi, -1 < z < 0). \quad (2.18)$$

The dynamic condition (2.13) and the kinematic condition (2.10) on  $TS(t)$  give

$$\varphi_0 = 0, \quad \frac{\partial \eta_0}{\partial t} = \frac{\partial \varphi_0}{\partial z} \quad (r > a/H, 0 \leq \theta < 2\pi, z = 0). \quad (2.19)$$

The dynamic condition (2.13) and the kinematic condition (2.11) on  $VS(t)$  give

$$\varphi_0 = -zt, \quad \frac{\partial h_0}{\partial t} = \frac{\partial \varphi_0}{\partial r} \quad (r = a/H, 0 \leq \theta < 2\pi, -1 < z < 0). \quad (2.20)$$

The condition (2.14) on  $BS(t)$  becomes

$$\frac{\partial \varphi_0}{\partial z} = 0 \quad (r > a/H, 0 \leq \theta < 2\pi, z = -1). \quad (2.21)$$

The initial conditions (2.15) at  $t = 0$  yield

$$\varphi_0(r, \theta, z, 0) = 0, \quad \eta_0(r, \theta, 0) = 0, \quad h_0(z, \theta, 0) = 0. \quad (2.22)$$

The condition at the far field (2.16) becomes

$$\varphi_0 \rightarrow 0 \quad (r \rightarrow +\infty). \quad (2.23)$$

The intersection of the rigid bottom and initially vertical free surface is the bottom circle of the cylindrical cavity  $r = a/H, 0 \leq \theta < 2\pi, z = -1$ . The vertical velocities on these surfaces should be equal at the bottom circle. By condition (2.20) we get  $\varphi_{0,z} = -t$  along the free surface of the cavity and by (2.21) we know  $\varphi_{0,z} = 0$  at the rigid bottom, which implies that the velocities do not match at the bottom circle. This indicates that singularity of the flow is expected at this circle within the mathematical model (2.18)-(2.23).

Fourier series method is used in solving (2.18)-(2.23). Due to the problem being axisymmetric, the velocity potential is dependent only on  $r, z$  and  $t$

$$\varphi_0(r, z, t) = 2t \sum_{n=0}^{\infty} \frac{(-1)^{n+1}}{\sigma_n^2} \frac{K_0(\sigma_n r)}{K_0(\sigma_n \frac{a}{H})} \sin(\sigma_n z), \quad (2.24)$$

where  $\sigma_n = \frac{\pi}{2}(2n + 1)$  and  $K_0(\sigma_n r)$  is the modified Bessel function of order zero of the second kind.

The vertical velocity on the top free surface,  $r > \frac{a}{H}, z = 0$ , is

$$\frac{\partial \varphi_0}{\partial z}(r, 0, t) = \frac{4t}{\pi} \sum_{n=0}^{\infty} \frac{(-1)^{n+1}}{2n + 1} \frac{K_0(\sigma_n r)}{K_0(\sigma_n \frac{a}{H})} \quad (2.25)$$

the radial velocity on the vertical free surface  $r = \frac{a}{H}, -1 < z < 0$ , is

$$\frac{\partial \varphi_0}{\partial r}\left(\frac{a}{H}, z, t\right) = \frac{4t}{\pi} \sum_{n=0}^{\infty} \frac{(-1)^{n+1}}{2n + 1} \frac{K_0'(\sigma_n \frac{a}{H})}{K_0(\sigma_n \frac{a}{H})} \sin(\sigma_n z), \quad (2.26)$$

and the radial velocity along the bottom,  $r > \frac{a}{H}, z = -1$ , is

$$\frac{\partial \varphi_0}{\partial r}(r, -1, t) = \frac{4t}{\pi} \sum_{n=0}^{\infty} \frac{1}{2n + 1} \frac{K_0'(\sigma_n r)}{K_0(\sigma_n \frac{a}{H})}. \quad (2.27)$$

By the integration of (2.25) with respect to  $t$  and by (2.19), the top free surface shape

$\eta_0(r, t)$  is expressed by

$$\eta_0(r, t) = \frac{2t^2}{\pi} \sum_{n=0}^{\infty} \frac{(-1)^{n+1} K_0(\sigma_n r)}{2n+1 K_0(\sigma_n \frac{a}{H})}. \quad (2.28)$$

Integration of (2.26) with respect to  $t$  and by the relation in (2.20), the vertical free surface shape  $h_0(z, t)$  is represented by the equation

$$h_0(z, t) = \frac{2t^2}{\pi} \sum_{n=0}^{\infty} \frac{(-1)^{n+1} K_0'(\sigma_n \frac{a}{H})}{2n+1 K_0(\sigma_n \frac{a}{H})} \sin(\sigma_n z). \quad (2.29)$$

### 2.3. Reduction to the 2-D problem

As the radius and the centre of the cavity approach infinity, the problem reduces to the classical two-dimensional dam break problem by Korobkin and Yilmaz (2009). Let  $a/H \rightarrow \infty$ ,  $r \rightarrow \infty$  and  $r - a/H = x$ . By (A.2), as  $\sigma_n r \rightarrow \infty$ ,

$$K_0(\sigma_n r) \sim \sqrt{\frac{\pi}{2\sigma_n r}} e^{-\sigma_n r}, \quad (2.30)$$

and as  $\sigma_n \frac{a}{H} \rightarrow \infty$ ,

$$K_0(\sigma_n \frac{a}{H}) \sim \sqrt{\frac{\pi}{2\sigma_n \frac{a}{H}}} e^{-\sigma_n \frac{a}{H}}. \quad (2.31)$$

In the limit, the velocity potential  $\varphi_0(x, z, t)$  in (2.24) becomes

$$\varphi_0(x, z, t) = 2t \sum_{n=0}^{\infty} \frac{(-1)^{n+1}}{\sigma_n^2} e^{-\sigma_n x} \sin(\sigma_n z)$$

and it corresponds to the velocity potential  $\varphi_0(x, y, t)$  in the 2 dimensional case.

## 2.4. Analysis of the singularity of the radial velocity at the bottom circle

In order to study the singularity of the radial velocity at the bottom circle it is convenient to separate  $\varphi_{0,r}(r, z, t)$  as follows

$$\varphi_{0,r}(r, z, t) = 2t \left( \sum_{n=0}^N \frac{(-1)^{n+1}}{\sigma_n} \frac{K'_0(\sigma_n r)}{K_0(\sigma_n \frac{a}{H})} \sin(\sigma_n z) + \sum_{n=N+1}^{\infty} \frac{(-1)^{n+1}}{\sigma_n} \frac{K'_0(\sigma_n r)}{K_0(\sigma_n \frac{a}{H})} \sin(\sigma_n z) \right), \quad (2.32)$$

where  $N$  is a large number. Substituting the large argument behaviour of the modified Bessel functions (2.30) and (2.31) in the second summation of (2.32), one gets

$$\varphi_{0,r}(r, z, t) \sim 2t \left( \sum_{n=0}^N \frac{(-1)^{n+1}}{\sigma_n} \frac{K'_0(\sigma_n r)}{K_0(\sigma_n \frac{a}{H})} \sin(\sigma_n z) + \sqrt{\frac{a}{Hr}} \sum_{n=N+1}^{\infty} \frac{(-1)^n}{\sigma_n} e^{-\sigma_n(r-\frac{a}{H})} \sin(\sigma_n z) \right). \quad (2.33)$$

The radial derivative (2.33) at the initially vertical free surface is

$$\begin{aligned} \varphi_{0,r} \left( \frac{a}{H}, z, t \right) &\sim 2t \sum_{n=0}^N \frac{(-1)^{n+1}}{\sigma_n} \frac{K'_0 \left( \sigma_n \frac{a}{H} \right)}{K_0 \left( \sigma_n \frac{a}{H} \right)} \sin(\sigma_n z) \\ &\quad + 2t \left( \sum_{n=0}^{\infty} \frac{(-1)^n}{\sigma_n} \sin(\sigma_n z) - \sum_{n=0}^N \frac{(-1)^n}{\sigma_n} \sin(\sigma_n z) \right) \\ &\sim \frac{2t}{\pi} \ln \left( \tan \frac{\pi}{4} (1 + z) \right). \end{aligned} \quad (2.34)$$

Therefore, as  $z \rightarrow -1$ , the singularity in the radial derivative of the leading order velocity is logarithmic at the bottom circle ( $r = a/H, z = -1$ ). Moreover, the singularity in  $\partial\varphi_0/\partial r$  in (2.34) is exactly the same as the singularity in  $\partial\varphi_0/\partial x$  in Korobkin and Yilmaz (2009). Therefore, the rest of the calculations for the inner region will be the same as in that paper.

The radial derivative (2.33) along the bottom is

$$\begin{aligned} \varphi_{0,r}(r, -1, t) &\sim 2t \sum_{n=0}^N \frac{1}{\sigma_n} \frac{K'_0(\sigma_n r)}{K_0(\sigma_n \frac{a}{H})} - 2t \sqrt{\frac{a}{Hr}} \left( \sum_{n=0}^{\infty} \frac{1}{\sigma_n} e^{-\sigma_n(r-\frac{a}{H})} - \sum_{n=0}^N \frac{1}{\sigma_n} e^{-\sigma_n(r-\frac{a}{H})} \right) \\ &\sim \frac{2t}{\pi} \sqrt{\frac{a}{Hr}} \ln \left( \tanh \frac{\pi}{4} \left( r - \frac{a}{H} \right) \right). \end{aligned} \quad (2.35)$$



As  $r \rightarrow a/H$ , the singularity in the radial derivative of the leading order velocity potential is logarithmic at the bottom circle ( $r = a/H, z = -1$ ). The horizontal velocity along the bottom in the 2-D problem is logarithmic singular too as  $x \rightarrow 0$ .

## 2.5. Numerical results

The numerical results of the radial velocity of the initially vertical free surface, the radial velocity along the rigid bottom and the free surface shapes for three different values  $a/H$  are presented in this section. When plotting the figures, the summation is truncated at  $n = 999$ . This value of  $n$  gives a relative error  $5 \times 10^{-4}$ . By (A.2), we know that  $K_m(w)$  decays as the argument  $w \rightarrow \infty$ . Ergo, to avoid the problems caused by the ratio of the modified Bessel functions for large arguments, which gives the ratio  $0/0$  in Matlab, we cut the summations at  $N = 220$  for the computation of the radial velocity along the initially vertical free surface,  $N = 442$  for the computation of the radial velocity along the rigid bottom and  $N = 110$  for the free surface shapes, and after that for the rest of terms, we use the asymptotic expansions for large arguments (A.2).

### 2.5.1. Velocities of the free surfaces

The analysis of the radial velocity at the bottom circle (Section 2.4) indicates that the radial velocity of the initially vertical free surface is log-singular there (see (2.34)). When plotting Figure 2.2, we use the differentiation property (A.8) and the asymptotic expansion for large arguments (A.2) for  $n > 220$ . The equation of the radial velocity (2.26) becomes

$$\begin{aligned} \frac{\partial \varphi_0}{\partial r} \left( \frac{a}{H}, z, t \right) &\approx \frac{4t}{\pi} \left( \sum_{n=0}^{220} \frac{(-1)^{n+1}}{2n+1} \frac{K_0'(\sigma_n \frac{a}{H})}{K_0(\sigma_n \frac{a}{H})} \sin(\sigma_n z) + \sum_{n=221}^{999} \frac{(-1)^{n+1}}{2n+1} \frac{K_0'(\sigma_n \frac{a}{H})}{K_0(\sigma_n \frac{a}{H})} \sin(\sigma_n z) \right) \\ &\approx \frac{-4t}{\pi} \left( \sum_{n=0}^{220} \frac{(-1)^{n+1}}{2n+1} \frac{K_1(\sigma_n \frac{a}{H})}{K_0(\sigma_n \frac{a}{H})} \sin(\sigma_n z) + \sum_{n=221}^{999} \frac{(-1)^{n+1}}{2n+1} \sin(\sigma_n z) \right). \end{aligned} \quad (2.36)$$

The values close to  $z = -1$ , for  $a/H = 0.5, 1, 2$  are shown in Table 2.1. From the table

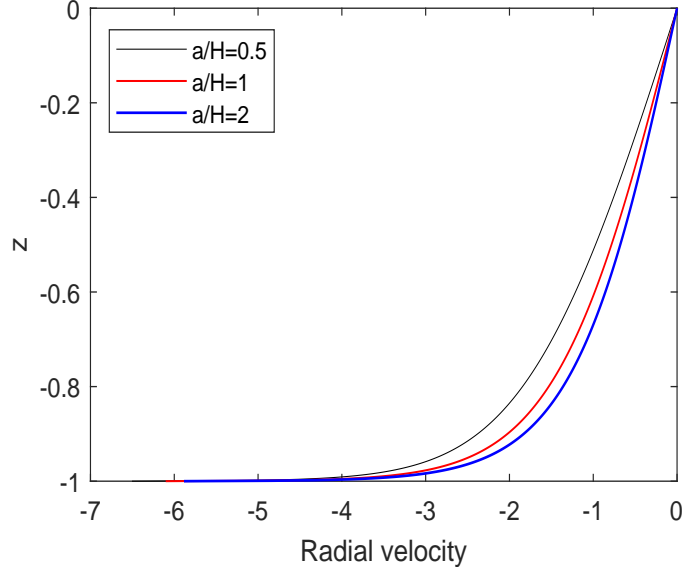


Figure 2.2. Radial velocity  $\varphi_{0,r}(a/H, z, t)$  of the initially vertical free surface for  $a/H = 0.5, 1, 2$ .

it is seen that the values increase rapidly in the negative direction as  $z \rightarrow -1$ . This result, which is expected because of the singularity, is also obvious in Fig. 2.2.

Table 2.1. Radial velocity of the initially vertical free surface

$z$	$\varphi_{0,r}(0.5, z, t)$	$\varphi_{0,r}(1, z, t)$	$\varphi_{0,r}(2, z, t)$
-0.998	-4.9518	-4.5497	-4.3318
-0.999	-5.4550	-5.0525	-4.8344
-1	-6.5045	-6.1020	-5.8838

The analysis of the radial velocity at the bottom circle shows that the radial velocity along the rigid bottom is log-singular too (see (2.35)). We truncate the sum (2.27), at  $N = 442$  and use the asymptotic expansion for large arguments of the modified Bessel functions (A.2) for bigger  $n$ . Therefore, the equation of the radial velocity plotted in

Figure 2.3 becomes

$$\begin{aligned} \frac{\partial \varphi_0}{\partial r}(r, -1, t) &\approx \frac{4t}{\pi} \left( \sum_{n=0}^{442} \frac{1}{2n+1} \frac{K_0'(\sigma_n r)}{K_0(\sigma_n \frac{a}{H})} + \sum_{n=443}^{999} \frac{1}{2n+1} \frac{K_0'(\sigma_n r)}{K_0(\sigma_n \frac{a}{H})} \right) \\ &\approx \frac{-4t}{\pi} \left( \sum_{n=0}^{442} \frac{1}{2n+1} \frac{K_1(\sigma_n r)}{K_0(\sigma_n \frac{a}{H})} + \sqrt{\frac{a}{Hr}} \sum_{n=443}^{999} \frac{1}{2n+1} e^{-\sigma_n(r-a/H)} \right). \end{aligned} \quad (2.37)$$

For  $a/H = 0.5, 1, 2$ , approaching closer to  $r = a/H$ , causes to the radial velocity values a

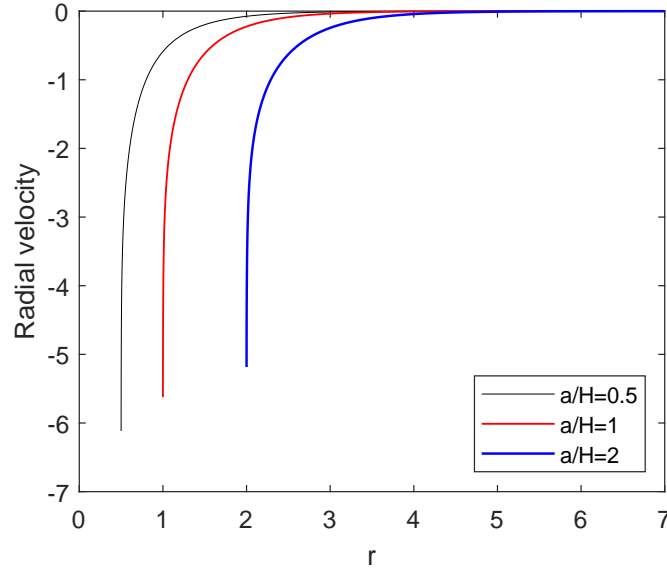


Figure 2.3. Radial velocity  $\varphi_{0,r}(r, -1, t)$  along the rigid bottom for  $a/H = 0.5, 1, 2$ .

quick increase in the negative direction (see Fig 2.3). This result is also provided in Table 2.2, which demonstrates the presence of singularities along the bottom circle.

## 2.5.2. Free surface shapes

The non-dimensional shapes of the top free surface (2.28) and the initially vertical free surface (2.29) for  $\varepsilon = 0.01$ ,  $t = 1$ , and different values of  $a/H$ , namely 0.5, 1 and 2, are shown by dashed lines in Figure 2.4 and Figure 2.5 respectively. When plotting the free surfaces, we truncate the sum at  $N = 110$ , because for bigger  $n$  we get the value 0/0

Table 2.2. Radial velocity along the rigid bottom

$r$	$\varphi_{0,z}(r, -1, t)$ $a/H = 0.5$	$\varphi_{0,z}(r, -1, t)$ $a/H = 1$	$\varphi_{0,z}(r, -1, t)$ $a/H = 2$
$a/H$	-6.1162	-5.6229	-5.1841
$a/H + 0.001$	-5.3399	-4.8777	-4.5282
$a/H + 0.002$	-4.9386	-4.5178	-4.2224

in Matlab, and use A.2 for bigger  $n$ . Thus, for the numerical computations, the equations of the free surfaces (2.28) and (2.29) become

$$\begin{aligned}\eta_0(r, t) &\approx \frac{2t^2}{\pi} \left( \sum_{n=0}^{110} \frac{(-1)^{n+1}}{2n+1} \frac{K_0(\sigma_n r)}{K_0(\sigma_n \frac{a}{H})} + \sum_{n=111}^{999} \frac{(-1)^{n+1}}{2n+1} \frac{K_0(\sigma_n r)}{K_0(\sigma_n \frac{a}{H})} \right) \\ &\approx \frac{2t^2}{\pi} \left( \sum_{n=0}^{110} \frac{(-1)^{n+1}}{2n+1} \frac{K_0(\sigma_n r)}{K_0(\sigma_n \frac{a}{H})} + \sqrt{\frac{a}{Hr}} \sum_{n=111}^{999} \frac{(-1)^{n+1}}{2n+1} e^{-\sigma_n(r-a/H)} \right),\end{aligned}$$

and

$$\begin{aligned}h_0(z, t) &\approx \frac{2t^2}{\pi} \left( \sum_{n=0}^{110} \frac{(-1)^{n+1}}{2n+1} \frac{K_0'(\sigma_n \frac{a}{H})}{K_0(\sigma_n \frac{a}{H})} \sin(\sigma_n z) + \sum_{n=111}^{999} \frac{(-1)^{n+1}}{2n+1} \frac{K_0'(\sigma_n \frac{a}{H})}{K_0(\sigma_n \frac{a}{H})} \sin(\sigma_n z) \right) \\ &\approx \frac{-2t^2}{\pi} \left( \sum_{n=0}^{110} \frac{(-1)^{n+1}}{2n+1} \frac{K_1(\sigma_n \frac{a}{H})}{K_0(\sigma_n \frac{a}{H})} \sin(\sigma_n z) + \sum_{n=111}^{999} \frac{(-1)^{n+1}}{2n+1} \sin(\sigma_n z) \right).\end{aligned}$$

respectively. It is seen that the top free surface deflects downwards near  $r = a/H$ , and the initially vertical free surface deflects to the left near  $z = -1$ .

For comparison, in these figures we also plot by solid line the shapes of the vertical free surface and horizontal free surface for the 2-dimensional case. Note that by increasing the ratio between  $a$  and  $H$ , the shapes get closer to the 2-dimensional case. Furthermore, from Section 2.3 we deduce that, as the ratio  $a/H$  and  $r$  go to infinity, with  $r - a/H = x$ , the shapes actually coincide.

To conclude, we proved analytically and numerically that the cylindrical cavity collapse treated in this chapter, is actually the 3-D generalization of the 2-D problem in Korobkin and Yilmaz (2009).

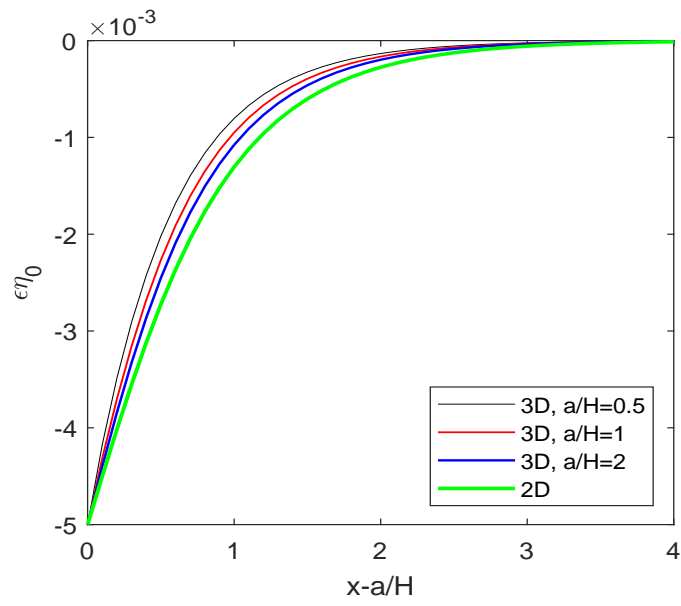


Figure 2.4. Top free surface at time  $t = 1$ ,  $\varepsilon = 0.01$ ,  $a/H = 0.5$ ,  $a/H = 1$ ,  $a/H = 2$  and 2D

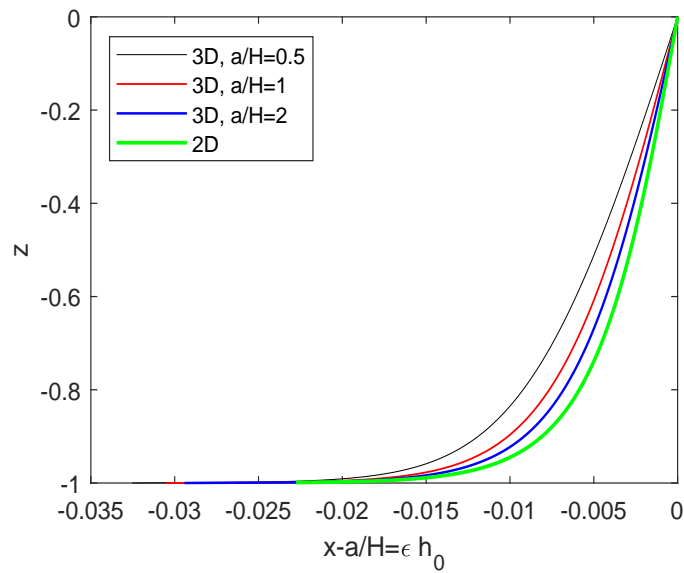


Figure 2.5. Vertical free surface at time  $t = 1$ ,  $\varepsilon = 0.01$ ,  $a/H = 0.5$ ,  $a/H = 1$ ,  $a/H = 2$  and 2D

## CHAPTER 3

### THE COLLAPSE OF A VERTICAL CYLINDRICAL CAVITY OF CIRCULAR CROSS SECTIONS EXTENDING FROM THE FREE SURFACE AND HAVING LESS DEPTH THAN A SURROUNDING FLUID OF FINITE DEPTH

We study the three dimensional unsteady problem of gravity-driven flow caused by instantly removing a cylinder from a deeper liquid region. Initially the fluid region  $\Omega'(0)$  lies outside the cylindrical cavity, extends to infinity in the radial direction and is bounded by the rigid bottom in the vertical direction. The problem is treated in cylindrical coordinates  $(r', \theta, z')$ . At time  $t' = 0$ , when the cylindrical cavity starts collapsing due to gravity, the liquid region is bounded by the following surfaces: the top free surface  $r' > a$ ,  $0 \leq \theta < 2\pi$ ,  $z' = H^+$ , the vertical free surface  $r' = a$ ,  $0 \leq \theta < 2\pi$ ,  $H^- < z' < H^+$ , the lower free surface  $r' < a$ ,  $0 \leq \theta < 2\pi$ ,  $z' = H^-$ , and by the rigid bottom  $z' = 0$ , where  $a$ ,  $H^+$  and  $H^-$  represent the radius of the cylinder, the liquid depth, and the distance between the lower disc of the cylinder and the rigid bottom respectively and the prime stands for the dimensional variables (see Fig. 3.1).

By the sudden collapse of the cylinder, due to the presence of gravity, the liquid starts flowing to the cavity. The liquid is incompressible and inviscid and the flow is potential. We are interested in the flow field and the free surface shapes at the initial stage of the process.

This problem is the generalized form of the two dimensional gravity-driven flow, which is caused by a sudden break of a thin vertical plate separating two immiscible fluids of different densities and depths studied by Yilmaz et al. (2013a). In the paper, the linear problem is solved by the Fourier series method and the aim is to determine the motion of the interface and the singular behaviour at the triple point and the corner point. The analysis of the local flow at the triple point, where the vertical free surface, the lower free surface and the interface meet, shows that the singularity depends on the density ratio and the shape of the flow region. The flow velocity at the corner point, where the interface

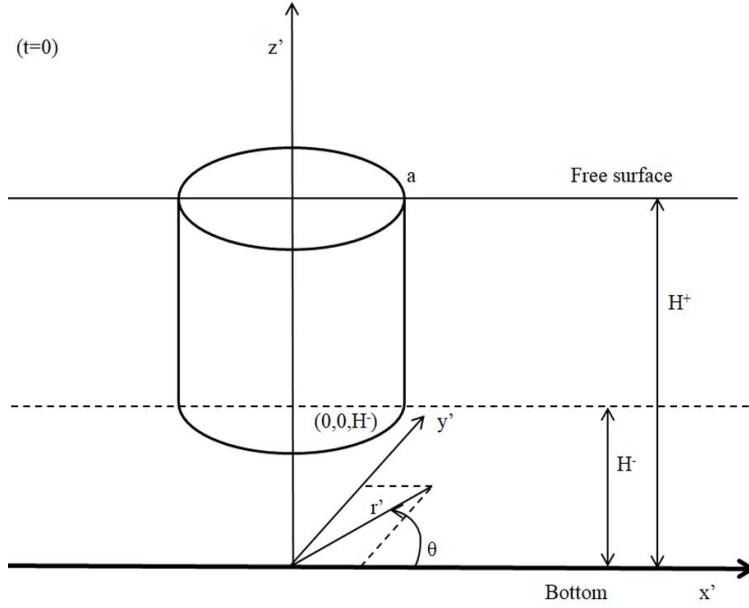


Figure 3.1. Flow region at initial time  $t' = 0$

and the rigid bottom meet, is log-singular for two liquids of different densities and non-singular otherwise. In this chapter, we apply similar techniques to the 3-D problem and analyse how the results match the linear problem in the 2-D case.

### 3.1. Formulation of the problem

The fluid motion is assumed to be irrotational. This implies the existence of a velocity potential  $\varphi'(r', \theta, z', t')$ , which by the incompressibility condition, satisfies Laplace's equation

$$\nabla^2 \varphi' = 0 \quad (\text{in } \Omega'(t')), \quad (3.1)$$

where  $\Omega'(t')$  is the flow region.

The kinematic condition on the free surface is that the fluid particles on the free surface remain on the free surface

$$\varphi'_{z'} = \varphi'_{r'} \eta'_{r'} + \frac{1}{r'^2} \varphi'_{\theta'} \eta'_{\theta'} + \eta'_{t'} \quad (\text{on } TS'(t')), \quad (3.2)$$

$$\varphi'_{r'} = \varphi'_{z'} \zeta'_{z'} + \frac{1}{r'^2} \varphi'_{\theta} \zeta'_{\theta} + \zeta'_{r'} \quad (\text{on } VS'(t')), \quad (3.3)$$

$$\varphi'_{z'} = \varphi'_{r'} \nu'_{r'} + \frac{1}{r'^2} \varphi'_{\theta} \nu'_{\theta} + \nu'_{r'} \quad (\text{on } LS'(t')). \quad (3.4)$$

Here  $TS'(t')$  represents the top free surface  $r' > a + \zeta'(z', \theta, t')$ ,  $0 \leq \theta < 2\pi$ ,  $z' = H^+ + \eta'(r', \theta, t')$ ,  $VS'(t')$  the vertical free surface  $r' = a + \zeta'(z', \theta, t')$ ,  $0 \leq \theta < 2\pi$ ,  $H^- + \nu'(a, \theta, t') < z' < H^+ + \eta'(a, \theta, t')$  and  $LS'(t')$  the lower free surface  $r' < a + \zeta'(z', \theta, t')$ ,  $0 \leq \theta < 2\pi$ ,  $z' = H^- + \nu'(r', \theta, t')$ , which have to be determined for small times.

The Bernoulli equation for unsteady irrotational flow is

$$-\frac{p'}{\rho_0} = \varphi'_{r'} + \frac{1}{2} |\nabla \varphi'|^2 + g(z' - H^+) \quad (r' \geq a), \quad (3.5)$$

$$-\frac{p'}{\rho_0} = \varphi'_{r'} + \frac{1}{2} |\nabla \varphi'|^2 + g(z' - H^-) \quad (r' < a). \quad (3.6)$$

The fluid is considered to be inviscid, implying that the pressure  $p$  at the free surface is the same as the atmospheric pressure  $p_0$

$$p' = 0 \quad (\text{on } FS'(t')), \quad (3.7)$$

where the notation  $FS'(t')$  stands for all free surfaces. Explicitly, the pressure on each free surface is

$$\varphi'_{r'} + \frac{1}{2} |\nabla \varphi'|^2 + g\eta'(r', \theta, t') = 0 \quad (\text{on } TS'(t')), \quad (3.8)$$

$$\varphi'_{r'} + \frac{1}{2} |\nabla \varphi'|^2 + g(z' - H^+) = 0 \quad (\text{on } VS'(t')), \quad (3.9)$$

$$\varphi'_{r'} + \frac{1}{2} |\nabla \varphi'|^2 + g\nu'(r', \theta, t') = 0 \quad (\text{on } LS'(t')). \quad (3.10)$$

The bottom surface  $BS'(t')$  is rigid. The boundary condition is that there is no velocity in  $z'$  direction at the bottom surface  $BS'(t')$

$$\varphi'_{z'} = 0 \quad (\text{on } BS'(t')). \quad (3.11)$$



Initially, before the cylinder collapses, the fluid is at rest and there is no deformation of the free surfaces

$$\varphi'(r', \theta, z', 0) = 0, \quad \eta'(r', \theta, 0) = 0, \quad \zeta'(z', \theta, 0) = 0, \quad \nu'(r', \theta, 0) = 0 \quad (t' = 0). \quad (3.12)$$

At  $r' = 0, 0 < z' < H^-$  the flow is bounded,

$$\varphi' \text{ is bounded.} \quad (3.13)$$

At infinity there is no fluid motion, so

$$\varphi' \rightarrow 0 \quad (r' \rightarrow +\infty). \quad (3.14)$$

In order to express the problem in dimensionless form, we introduce the non-dimensional variables

$$\begin{aligned} r' &= rH^+, \quad z' = zH^+, \quad t' = Tt, \\ \varphi' &= gH^+T\varphi, \quad p' = \rho_0gH^+p, \quad T = \varepsilon^{1/2}\sqrt{H^+/g} \\ \eta' &= S_1\eta, \quad \zeta' = S_2\zeta, \quad \nu' = S_3\nu, \\ S_1/H^+ &= \mathcal{O}(\varepsilon), \quad S_2/H^+ = \mathcal{O}(\varepsilon), \quad S_3/H^+ = \mathcal{O}(\varepsilon). \end{aligned} \quad (3.15)$$

Replacing (3.15) in the boundary value problem (3.1)-(3.14), the nondimensional potential  $\varphi(r, \theta, z, t)$  satisfies the following equations:

$$\nabla^2\varphi = 0 \quad (\text{in } \Omega(t)) \quad (3.16)$$

$$\varphi_z = \varepsilon\varphi_r\eta_r + \frac{\varepsilon}{r^2}\varphi_\theta\eta_\theta + \eta_t \quad (\text{on } TS(t)), \quad (3.17)$$

$$\varphi_r = \varepsilon\varphi_z\zeta_z + \frac{\varepsilon}{r^2}\varphi_\theta\zeta_\theta + \zeta_t \quad (\text{on } VS(t)), \quad (3.18)$$

$$\varphi_z = \varepsilon\varphi_r\nu_r + \frac{\varepsilon}{r^2}\varphi_\theta\nu_\theta + \nu_t \quad (\text{on } LS(t)), \quad (3.19)$$

$$p = \varphi_t + \frac{1}{2}\varepsilon|\nabla\varphi|^2 + z - 1 \quad (r \geq a/H^+), \quad (3.20)$$

$$p = \varphi_t + \frac{1}{2}\varepsilon|\nabla\varphi|^2 + z - \delta \quad (r < a/H^+), \quad (3.21)$$

$$p = 0 \quad (\text{on } FS(t)) \quad (3.22)$$

$$\varphi_t + \frac{1}{2}\varepsilon|\nabla\varphi|^2 + \varepsilon\eta(r, \theta, t, \varepsilon) = 0 \quad (\text{on } TS(t)) \quad (3.23)$$

$$\varphi_t + \frac{1}{2}\varepsilon|\nabla\varphi|^2 + z - 1 = 0 \quad (\text{on } VS(t)) \quad (3.24)$$

$$\varphi_t + \frac{1}{2}\varepsilon|\nabla\varphi|^2 + \varepsilon\nu(r, \theta, t, \varepsilon) = 0 \quad (\text{on } LS(t)) \quad (3.25)$$

$$\varphi_z = 0 \quad (\text{on } BS(t)), \quad (3.26)$$

$$\varphi(r, \theta, z, 0, \varepsilon) = 0, \quad \eta(r, \theta, 0, \varepsilon) = 0, \quad \zeta(z, \theta, 0, \varepsilon) = 0, \quad \nu(r, \theta, 0, \varepsilon) = 0 \quad (t = 0) \quad (3.27)$$

$$\varphi - \text{bounded} \quad (r = 0, 0 < z < \delta) \quad (3.28)$$

$$\varphi \rightarrow 0 \quad (r \rightarrow +\infty) \quad (3.29)$$

Here  $\Omega(t)$  is the flow region, which is bounded by the free surface  $FS(t)$  and the bottom surface  $BS(t)$   $z = 0$ .  $FS(t)$  is composed by the union of the top free surface  $TS(t)$ :  $r > a/H^+ + \varepsilon\zeta(z, \theta, t, \varepsilon)$ ,  $0 \leq \theta < 2\pi$ ,  $z = 1 + \varepsilon\eta(r, \theta, t, \varepsilon)$ , the vertical free surface  $VS(t)$ :  $r = a/H^+ + \varepsilon\zeta(z, \theta, t, \varepsilon)$ ,  $0 \leq \theta < 2\pi$ ,  $\delta + \varepsilon\nu(a/H^+, \theta, t, \varepsilon) < z < 1 + \varepsilon\eta(a/H^+, \theta, t, \varepsilon)$  and the lower free surface  $LS(t)$ :  $r < a/H^+ + \varepsilon\zeta(z, \theta, t, \varepsilon)$ ,  $0 \leq \theta < 2\pi$ ,  $z = \delta + \varepsilon\nu(r, \theta, t, \varepsilon)$ , which have to be determined for small times. The new parameter  $\delta$  represents the depth ratio  $H^-/H^+$ .

We shall now suppose that the velocity potential and the free surface displacements are small, by searching for a solution of (3.16)-(3.29), as  $\varepsilon \rightarrow 0$  in the form

$$\begin{aligned} \varphi(r, \theta, z, t, \varepsilon) &= \varphi_0(r, \theta, z, t) + \varepsilon\varphi_1(r, \theta, z, t) + \mathcal{O}(\varepsilon^2), \\ \eta(r, \theta, t, \varepsilon) &= \eta_0(r, \theta, t) + \varepsilon\eta_1(r, \theta, t) + \mathcal{O}(\varepsilon^2), \\ \zeta(z, \theta, t, \varepsilon) &= \zeta_0(z, \theta, t) + \varepsilon\zeta_1(z, \theta, t) + \mathcal{O}(\varepsilon^2), \\ \nu(r, \theta, t, \varepsilon) &= \nu_0(r, \theta, t) + \varepsilon\nu_1(r, \theta, t) + \mathcal{O}(\varepsilon^2). \end{aligned} \quad (3.30)$$

### 3.1.1. Leading-order outer problem

The flow region  $\Omega(t)$  is split into two regions,  $\Omega^+(t)$  representing the exterior region:  $r > a/H^+, 0 \leq \theta < 2\pi, 0 < z < 1 + \varepsilon\eta(r, \theta, t, \varepsilon)$  and  $\Omega^-(t)$  the interior region  $r < a/H^+, 0 \leq \theta < 2\pi, 0 < z < \delta + \varepsilon\nu(r, \theta, t, \varepsilon)$ . So the exterior region is outside the cylinder, extending to the infinity in the radial direction and the interior region is underneath the cylinder and bounded. Substituting the asymptotic expansions (3.30) in the boundary value problem (3.16)-(3.29), as  $\varepsilon \rightarrow 0$  we get the exterior and the interior region boundary-value problem for the leading-order velocity potentials  $\varphi_0^+$  and  $\varphi_0^-$ . The Laplace's equation (3.16) in the exterior region becomes

$$\nabla^2 \varphi_0^+ = 0 \quad (r > a/H^+, 0 \leq \theta < 2\pi, 0 < z < 1). \quad (3.31)$$

The dynamic boundary condition (3.23) and the kinematic condition (3.17) on the top free surface yield

$$\varphi_0^+ = 0, \quad \frac{\partial \eta_0}{\partial t} = \frac{\partial \varphi_0^+}{\partial z} \quad (r > a/H^+, 0 \leq \theta < 2\pi, z = 1). \quad (3.32)$$

Equation (3.24) and (3.18) on the vertical free surface become

$$\varphi_0^+ = (1 - z)t, \quad \frac{\partial \zeta_0}{\partial t} = \frac{\partial \varphi_0^+}{\partial r} \quad (r = a/H^+, 0 \leq \theta < 2\pi, \delta < z < 1). \quad (3.33)$$

The condition at the rigid bottom (3.26) for the exterior region is

$$\frac{\partial \varphi_0^+}{\partial z} = 0 \quad (r \geq a/H^+, 0 \leq \theta < 2\pi, z = 0). \quad (3.34)$$

The initial conditions (3.27) become

$$\varphi_0^+(r, \theta, z, 0) = 0, \quad \eta_0(r, \theta, 0) = 0, \quad \zeta_0(z, \theta, 0) = 0 \quad (t = 0). \quad (3.35)$$

The condition at the far field (3.29) is

$$\varphi_0^+ \rightarrow 0 \quad (r \rightarrow +\infty). \quad (3.36)$$

Similarly, we obtain the interior region boundary-value problem for the leading-order velocity potential  $\varphi_0^-$ . The Laplace's equation (3.16) in the interior region becomes

$$\nabla^2 \varphi_0^- = 0 \quad (r < a/H^+, 0 \leq \theta < 2\pi, 0 < z < \delta). \quad (3.37)$$

The dynamic boundary condition (3.25) and the kinematic condition (3.19) on the lower free surface yield

$$\varphi_0^- = 0, \quad \frac{\partial v_0}{\partial t} = \frac{\partial \varphi_0^-}{\partial z} \quad (r < a/H^+, 0 \leq \theta < 2\pi, z = \delta). \quad (3.38)$$

The condition at the rigid bottom (3.16) for the interior region becomes

$$\frac{\partial \varphi_0^-}{\partial z} = 0 \quad (r < a/H^+, 0 \leq \theta < 2\pi, z = 0). \quad (3.39)$$

By (3.27) the initial conditions are

$$\varphi_0^-(r, \theta, z, 0) = 0, \quad v_0(r, \theta, 0) = 0 \quad (t = 0). \quad (3.40)$$

The velocity potential is bounded at the vertical axes (3.28), therefore

$$\varphi_0^-(0, \theta, z, t) \quad \text{bounded} \quad (r = 0). \quad (3.41)$$

The conditions at the interface of the two regions are that the pressures of the fluid are equal

$$\frac{\partial \varphi_0^+}{\partial t} - 1 = \frac{\partial \varphi_0^-}{\partial t} - \delta \quad (r = a/H^+, 0 \leq \theta < 2\pi, 0 < z < \delta), \quad (3.42)$$

and the radial velocities too

$$\frac{\partial \varphi_0^+}{\partial r} = \frac{\partial \varphi_0^-}{\partial r} \quad (r = a/H^+, 0 \leq \theta < 2\pi, 0 < z < \delta). \quad (3.43)$$

The intersection of the initially vertical free surface and lower horizontal free surface is the circle  $(a/H^+, \theta, \delta)$ , where  $0 \leq \theta < 2\pi$ . However, the conditions (3.33) and (3.38) along these surfaces do not match at this circle, thereupon singularity of the flow within the mathematical model (3.31)-(3.43) is expected there.

### 3.2. Solution by the Fourier series method

The boundary value problems in the exterior region (3.31)-(3.36) and in the interior region (3.37)-(3.41) are considered. We would like to find solutions in the form of an infinite linear combination of separated solutions, i.e.,  $\varphi_0^\pm = R^\pm(r)\Theta^\pm(\theta)Z^\pm(z)$ . By virtue of the problems being axisymmetric, there is no  $\theta$  dependence. The velocity potentials for the exterior and interior regions are given below:

$$\varphi_0^+ = t \sum_{n=0}^{\infty} c'_n K_0(\sigma_n r) \cos(\sigma_n z) \quad (3.44)$$

$$\varphi_0^- = t \sum_{n=0}^{\infty} d'_n I_0\left(\frac{\sigma_n r}{\delta}\right) \cos\left(\frac{\sigma_n z}{\delta}\right), \quad (3.45)$$

where  $\sigma_n = (2n + 1)(\pi/2)$ .  $I_0$  and  $K_0$  are the modified Bessel functions of the first and the second kind of order zero respectively. Note that the dynamic condition (3.33) is not yet applied. It will be used afterwards, together with the interface conditions (3.42) and (3.43), in order to determine the coefficients  $c'_n$  and  $d'_n$ . For calculation purposes, we introduce two new variables  $c_n = c'_n K_0(\sigma_n a/H^+)$  and  $d_n = d'_n I_0(\sigma_n(a/H^+)/\delta)$ , so that

(3.44) and (3.45) become:

$$\varphi_0^+ = t \sum_{n=0}^{\infty} c_n \frac{K_0(\sigma_n r)}{K_0(\sigma_n a/H^+)} \cos(\sigma_n z) \quad (3.46)$$

$$\varphi_0^- = t \sum_{n=0}^{\infty} d_n \frac{I_0\left(\frac{\sigma_n r}{\delta}\right)}{I_0\left(\frac{\sigma_n a/H^+}{\delta}\right)} \cos\left(\frac{\sigma_n z}{\delta}\right). \quad (3.47)$$

Replacing the velocity potentials (3.46) and (3.47) at the interface conditions (3.42) and (3.43), for  $r = a/H^+$  and  $0 < z < \delta$ , yields:

$$\sum_{n=0}^{\infty} c_n \cos(\sigma_n z) - 1 = \sum_{n=0}^{\infty} d_n \cos\left(\frac{\sigma_n z}{\delta}\right) - \delta, \quad (3.48)$$

$$-\sum_{n=0}^{\infty} c_n \sigma_n \frac{K_1(\sigma_n a/H^+)}{K_0(\sigma_n a/H^+)} \cos(\sigma_n z) = \sum_{n=0}^{\infty} d_n \frac{\sigma_n}{\delta} \frac{I_1\left(\frac{\sigma_n a/H^+}{\delta}\right)}{I_0\left(\frac{\sigma_n a/H^+}{\delta}\right)} \cos\left(\frac{\sigma_n z}{\delta}\right). \quad (3.49)$$

Multiplying (3.46) by  $\cos(\sigma_m z)$  and integrating with respect to  $z$  from 0 to 1, using (3.48) and (3.33), we get the first relation between  $c_n$  and  $d_n$ :

$$\frac{c_n}{2} - \sum_{m=0}^{\infty} \alpha_{nm} d_m = f_n, \quad \frac{\sigma_m}{\delta} \neq \sigma_n, \quad n = 0, 1, \dots \quad (3.50)$$

$$\frac{c_n}{2} - \frac{\delta}{2} d_n = f_n, \quad \frac{\sigma_m}{\delta} = \sigma_n, \quad n = 0, 1, \dots \quad (3.51)$$

where

$$f_n = \frac{\cos(\sigma_n \delta)}{\sigma_n^2}, \quad (3.52)$$

$$\alpha_{nm} = -(-1)^m \frac{\sigma_m \cos(\sigma_n \delta)/\delta}{\sigma_n^2 - \sigma_m^2/\delta^2}. \quad (3.53)$$

Multiplying (3.49) by  $\cos(\sigma_m z/\delta)$  and integrating with respect to  $z$  from 0 to  $\delta$ , we get the second relation between  $c_n$  and  $d_n$ :

$$-\sum_{n=0}^{\infty} c_n \sigma_n \frac{K_1(\sigma_n a/H^+)}{K_0(\sigma_n a/H^+)} \alpha_{nm} = d_m \frac{\sigma_m}{2} \frac{I_1\left(\frac{\sigma_m a/H^+}{\delta}\right)}{I_0\left(\frac{\sigma_m a/H^+}{\delta}\right)}, \quad \frac{\sigma_m}{\delta} \neq \sigma_n, \quad m = 0, 1, \dots \quad (3.54)$$

$$-c_m \frac{K_1(\sigma_m a/H^+)}{K_0(\sigma_m a/H^+)} = \frac{d_m}{\delta} \frac{I_1\left(\frac{\sigma_m a/H^+}{\delta}\right)}{I_0\left(\frac{\sigma_m a/H^+}{\delta}\right)}, \quad \frac{\sigma_m}{\delta} = \sigma_n, \quad m = 0, 1, \dots \quad (3.55)$$

Truncating the series in (3.50) up to  $M$  and the series in (3.54) up to  $N$  and replacing  $c_n$  in (3.54) by (3.50), we get the following system:

$$\sum_{l=0}^M \left[ \frac{\sigma_l}{2} \delta_{lm} \frac{I_1\left(\frac{\sigma_l a/H^+}{\delta}\right)}{I_0\left(\frac{\sigma_l a/H^+}{\delta}\right)} + 2 \sum_{n=0}^N \sigma_n \alpha_{nm} \alpha_{nl} \frac{K_1(\sigma_n a/H^+)}{K_0(\sigma_n a/H^+)} \right] d_l = -2g_m, \quad \frac{\sigma_m}{\delta} \neq \sigma_n, \quad (3.56)$$

where

$$g_m = \sum_{n=0}^N \frac{\alpha_{nm}}{\sigma_n} \cos(\sigma_n \delta) \frac{K_1(\sigma_n a/H^+)}{K_0(\sigma_n a/H^+)}, \quad (3.57)$$

$m = 0, 1, \dots, M$ , and  $\delta_{lm} = 1$  for  $l = m$  and  $\delta_{lm} = 0$  otherwise. By combining (3.51) and (3.55), we get

$$\left( \frac{\delta}{2} + \frac{1}{2\delta} \frac{I_1\left(\frac{\sigma_m a/H^+}{\delta}\right)}{I_0\left(\frac{\sigma_m a/H^+}{\delta}\right)} \right) d_m = -f_m \frac{K_1(\sigma_m a/H^+)}{K_0(\sigma_m a/H^+)}, \quad \frac{\sigma_m}{\delta} = \sigma_n, \quad m = 0, 1, \dots, M. \quad (3.58)$$

Solution to the systems (3.56) and (3.58) provides us with the coefficients  $d_l$ , which subsequently are used in obtaining the coefficients  $c_n$  in (3.50) and (3.51) for the cases  $\sigma_n \neq \sigma_m/\delta$  and  $\sigma_n = \sigma_m/\delta$  respectively. Note that the equations (3.48) and (3.50) correspond to (14) and (16) in Yilmaz et al. (2013a) for the case  $\gamma = 1$  and  $\sigma_n \neq \sigma_m/\delta$ . Furthermore, the equations (3.49), (3.54) and (3.56) reduce to (15), (19) and (20) in Yilmaz et al. (2013a) in a sense that is explained specifically in Sec. 3.3.

### 3.3. Reduction to the 2-D problem

As the radius and the center of cavity approach infinity, the problem reduces to the two dimensional dam-break flow of two immiscible fluids studied by Yilmaz et al. (2013a), for the particular case of density ratio  $\gamma = 1$ . For  $a/H^+ \rightarrow \infty$ , the asymptotic expansion for large arguments of the modified Bessel function of the first and second kind of first order (A.1) and (A.2) are

$$I_m\left(\frac{\sigma_n a/H^+}{\delta}\right) \sim \sqrt{\frac{1}{2\pi\sigma_n(a/H^+)/\delta}} e^{\sigma_n(a/H^+)/\delta} \quad (3.59)$$

and

$$K_m(\sigma_n a/H^+) \sim \sqrt{\frac{\pi}{2}} \frac{e^{-\sigma_n a/H^+}}{(\sigma_n a/H^+)^{1/2}}. \quad (3.60)$$

Replacing (3.59) and (3.60) in (3.49), the second condition at the interface becomes

$$-\sum_{n=0}^{\infty} c_n \sigma_n \cos(\sigma_n z) = \sum_{n=0}^{\infty} d_n \frac{\sigma_n}{\delta} \cos\left(\frac{\sigma_n z}{\delta}\right), \quad (3.61)$$

which is exactly the same as the second condition at the interface, see equation (15) in the 2-D problem in Yilmaz et al. (2013a). Note that the first condition at the interface (3.48) is same as the first condition at the interface, see equation (14) in Yilmaz et al. (2013a). To conclude, as  $a/H^+ \rightarrow \infty$ , the conditions at the interface of the 3-D problem match the conditions at the interface of the 2-D problem, implying that the solution of the systems will be same too.

### 3.4. Singularity analysis near the bottom circle

Due to the axisymmetric nature of the problem, it is sufficient to analyse the problem in the  $\tilde{x}\tilde{y}\tilde{z}$  coordinate system, which is obtained first by shifting the  $xyz$  coordinates in the  $xy$  plane by  $a/H^+ \cos \theta$  and  $a/H^+ \sin \theta$  in  $x$  and  $y$  directions respectively, and then by rotating the coordinates in the  $z$  direction by  $\theta$ , where  $\theta$  is arbitrary (see Fig. 3.2).

The relation between the new coordinates  $\tilde{x}\tilde{y}\tilde{z}$  and  $xyz$  is given as

$$\tilde{x} = \cos \theta \left(x - \frac{a}{H^+} \cos \theta\right) + \sin \theta \left(y - \frac{a}{H^+} \sin \theta\right) \quad (3.62)$$

$$\tilde{y} = -\sin \theta \left(x - \frac{a}{H^+} \cos \theta\right) + \cos \theta \left(y - \frac{a}{H^+} \sin \theta\right) \quad (3.63)$$

$$\tilde{z} = z. \quad (3.64)$$

The problem is independent of  $\theta$ , because of its axisymmetrical geometry. For simplicity, let  $\theta = 0$ . Notice that, for such value, the shift is only  $a/H^+$  in the  $x$  direction and there is



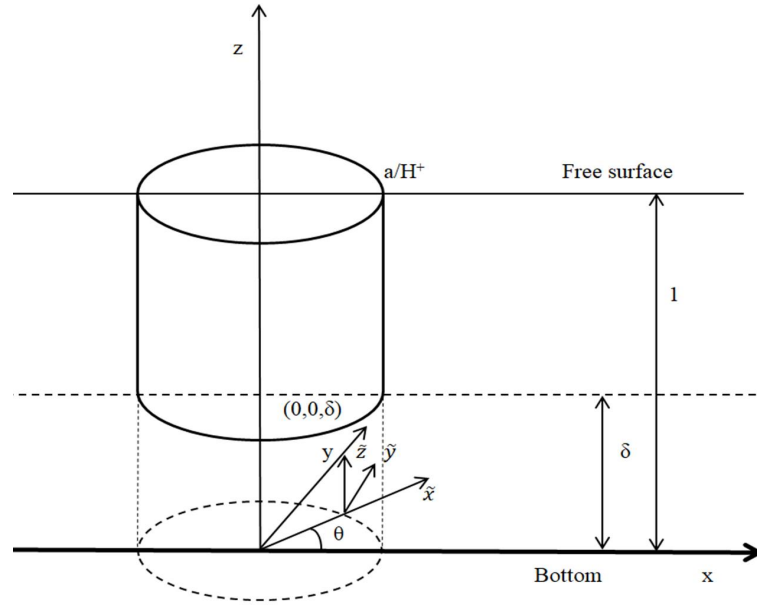


Figure 3.2. Shift from  $xyz$  to  $\tilde{x}\tilde{y}\tilde{z}$  coordinate system

no rotation, therefore

$$\tilde{x} = x - \frac{a}{H^+} \quad (3.65)$$

$$\tilde{y} = y \quad (3.66)$$

$$\tilde{z} = z. \quad (3.67)$$

In order to study the problem in the  $\tilde{x}\tilde{z}$  plane,  $\tilde{y}$  is taken to be 0 (see Fig. 3.3). Near the triple point  $\tilde{x} = 0$ ,  $\tilde{z} = \delta$ , we place a local polar coordinate system, so that the problem becomes identical to the boundary value problem describing the local flow at the triple point in Yilmaz et al. (2013a). Therefore,

$$\tilde{x} = \tilde{r} \cos \tilde{\theta} \quad (3.68)$$

$$\tilde{z} = \tilde{r} \sin \tilde{\theta} + \delta, \quad (3.69)$$

where  $\tilde{r}, \tilde{\theta}$  are local polar coordinates. The velocity potential satisfies the Laplace equation

in the local region and the following boundary conditions

$$\varphi_0\left(\tilde{r}, \frac{\pi}{2}\right) = 1 - \tilde{r} \sin \tilde{\theta} - \delta \quad (\tilde{r} > 0, \tilde{\theta} = \pi/2), \quad (3.70)$$

$$\varphi_0(\tilde{r}, -\pi) = 0 \quad (\tilde{r} > 0, \tilde{\theta} = -\pi). \quad (3.71)$$

The general solution can be written as

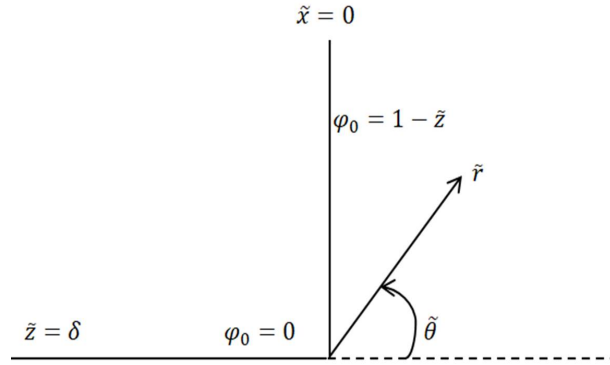


Figure 3.3. Boundary value problem describing the local flow near the bottom circle.

$$\varphi_0(\tilde{r}, \tilde{\theta}) = C \sin\left(\frac{2}{3}(\pi + \tilde{\theta})\right)\tilde{r}^{2/3} + \frac{2}{3}(1 - \delta)\left(1 + \frac{\tilde{\theta}}{\pi}\right) - \tilde{r} \sin \tilde{\theta}. \quad (3.72)$$

The horizontal and vertical velocities are

$$u = \frac{2}{3}C \sin\left(\frac{1}{3}(2\pi - \tilde{\theta})\right)\tilde{r}^{-1/3} - \frac{2(1 - \delta)}{3\pi} \sin \tilde{\theta} \tilde{r}^{-1} \quad (3.73)$$

and

$$v = \frac{2}{3}C \cos\left(\frac{1}{3}(2\pi - \tilde{\theta})\right)\tilde{r}^{-1/3} + \frac{2(1 - \delta)}{3\pi} \cos \tilde{\theta} \tilde{r}^{-1} - 1. \quad (3.74)$$

Thus, the flow velocity is  $\tilde{r}^{-1/3}$  singular at the triple point  $\tilde{x} = 0, \tilde{z} = \delta$ . Note that (3.73) and (3.74) correspond to the velocities  $u$  and  $v$  near the corner point, see equation (25) in Yilmaz et al. (2013a).

### 3.5. Nonlinear analysis at the bottom circle

The analysis of the flow near the bottom circle, shows that the outer solution is singular at  $x = a/H^+$ ,  $z = \delta$ . An inner solution is needed in order to describe the flow at this circle. The non-linear analysis of the initial stage of dam-break flow of two immiscible fluids is studied by Yilmaz et al. (2013b). Here the inner solution describes a jet flow formation at the corner point  $x = 0$ ,  $y = \delta$ . Similarly, due to the axisymmetric nature of the problem, and using the explanations from Section 3.4, it can be concluded that the nonlinear analysis of the 3-D problem will be same to the one in Yilmaz et al. (2013b).

### 3.6. Numerical results

Based on the local analysis at the bottom circle of the cavity (Section 3.4), it is of interest investigating numerically the radial and vertical velocities along the interface, particularly near the bottom circle. It is also significant to check numerically the radial velocity of the initially vertical free surface, the vertical velocity of the lower free surface and their behaviour near the bottom circle. On the other side, considering the conclusions of the limiting case (Section 3.3), it is of importance checking numerically how an increase in the ratio  $a/H^+$  affects the free surface shapes. In order to get these numerical results, first we should decide about the truncations of the series (3.50) and (3.54), namely we should find a suitable  $M$  and  $N$ , which guarantees the convergence of the solution. Hudde and Letens (1985)'s study on a sound propagating through a circular duct with a change in radius, suggests that  $N_A/N_B = R_A/R_B$ , where  $N_A$  is the number of the modes in the smaller duct,  $N_B$  is the number of modes in the larger duct,  $R_A$  and  $R_B$  are the radii of the smaller and larger duct respectively. Therefore, in our problem the number of modes  $N$  and  $M$  must be chosen such that  $N/M = \delta$ . During these analyses  $M = 999$  and  $N = 1999$ . While computing the radial velocity of the initially vertical free surface, we cut the series at  $n = 140$  and for bigger  $n$ , we use the asymptotic expansion for large arguments of the modified Bessel function of first kind (A.1), in order to avoid getting the result  $0/0$  from the Matlab code. Similarly, to avoid getting  $\infty/\infty$  while calculating the vertical velocity of the lower free surface, we truncate the series at  $m = 70$  and use the asymptotic expansion for large arguments for the modified Bessel function of the second

kind (A.2).

### 3.6.1. Convergence of the coefficients

Before introducing the numerical results about the velocities near the bottom circle of the cavity and the free surface shapes, it is crucial to check the convergence of the coefficients  $d_m$  and  $c_n$  on which these numerical results depend. Here  $H^+ = 2$ ,  $H^- = 1$  and  $a = 1$ . For different  $m$  and  $n$ , some values  $d_m$  and  $c_n$  are presented in Table 3.1 and Table 3.2 respectively.

Table 3.1. Convergence of  $d_m$

$d_m$	$m = 10, n = 20$	$m = 60, n = 120$	$m = 100, n = 200$	$m = 999, n = 1999$
$d_0$	-0.2591	-0.2590	-0.2590	-0.2590
$d_1$	0.0424	0.0423	0.0423	0.0423
$d_2$	-0.0185	-0.0183	-0.0183	-0.0183
...	...	...	...	...
$d_9$	0.0029	0.0020	0.0020	0.0020
...	...	...	...	...
$d_{19}$		0.0006	0.0006	0.0006

Table 3.2. Convergence of  $c_n$

$c_n$	$m = 10, n = 20$	$m = 60, n = 120$	$m = 100, n = 200$	$m = 999, n = 1999$
$c_0$	0.4077	0.4077	0.4077	0.4077
$c_1$	-0.1450	-0.1448	-0.1448	-0.1448
$c_2$	-0.0203	-0.0202	-0.0202	-0.0202
...	...	...	...	...
$c_9$	-0.0067	-0.0064	-0.0064	-0.0064
...	...	...	...	...
$c_{19}$	0.0031	0.0019	0.0019	0.0019

Note that the convergence is achieved for  $m = 60$  and  $n = 120$  with  $\epsilon_d = |d_{m_{999}} - d_{m_{60}}| \leq 10^{-5}$  and  $\epsilon_c = |c_{n_{1999}} - c_{n_{120}}| \leq 10^{-5}$ .

### 3.6.2. Radial and vertical velocities along the interface

We present the graphs of the radial and vertical velocities along the interface. The radial velocities match along the interface (see Fig. 3.4), as given in condition (3.43). Near  $z = 0$ , the radial velocities match well. Near  $z = 0.5$ , we don't have a good match,

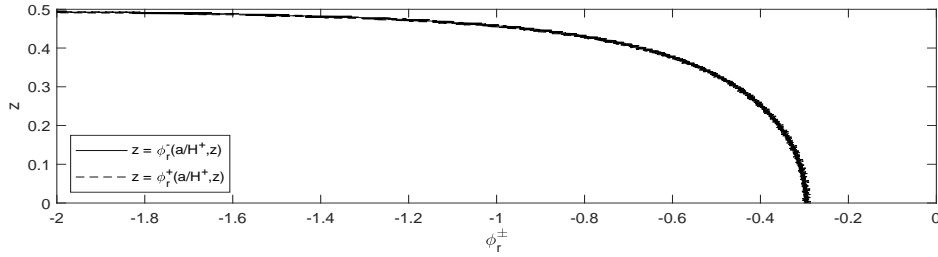


Figure 3.4. Radial velocities  $\phi_r^\pm(a/H^+, z)$  of the interface for  $\delta = 0.5$ .

which is expected because of the singularity (see Table 3.3). We notice that the radial velocity of the interface in Fig. 3.4 is same to the horizontal velocity of the interface for two liquids of same density presented in Fig. 6b in Yilmaz et al. (2013a).

Table 3.3. Radial velocities along the interface

$z$	$\varphi_{0,r}^+(0.5, z, t)$	$\varphi_{0,r}^-(0.5, z, t)$
0.001	-0.299007952532956	-0.297335981885625
0.002	-0.294524410147874	-0.291907829689814
0.003	-0.302225612780784	-0.294141517569342
...	...	...
0.497	2.407075121010925	-2.925394395518511
0.498	-2.521740351904609	-3.601924711771231
0.499	-4.603360133751212	-3.016350936808655

The vertical velocities match at the interface (see Fig. 3.5), satisfying so the condition (3.42). Near  $z = 0$ , we have a good match for  $\phi_z^\pm$ . Near  $z = 0.5$ , we do not have a good match, implying the existence of a singularity at  $(a/H^+, \delta)$  (see Table 3.4). As stated in Yilmaz et al. (2013a), we also notice that the vertical velocities match better than the

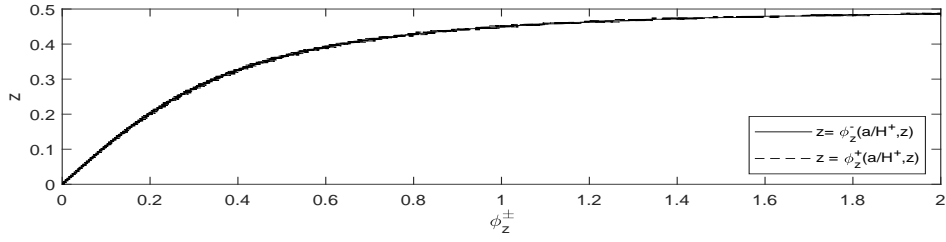


Figure 3.5. Vertical velocities  $\phi_z^\pm$  of the interface for  $\delta = 0.5$ .

radial ones. The graph in Fig. 3.5 is same to the one in Fig. 7b from the latter paper, which presents the vertical velocities along the interface for  $\delta = 0.5$  and the liquids have same density.

Table 3.4. Vertical velocities along the interface

$z$	$\varphi_{0,z}^+(0.5, z, t)$	$\varphi_{0,z}^-(0.5, z, t)$
0.001	0.005737873916772	0.005710282392787
0.002	0.003394409241131	0.003406804668442
0.003	-0.001520014346943	-0.001602789056567
...	...	...
0.497	3.865883515111893	3.509921204998019
0.498	4.417637283631854	4.986310683399990
0.499	8.257112982399617	7.252958347160366

### 3.6.3. Velocities of the free surfaces

Next, we calculate the radial velocity of the initially vertical free surface. The equation of the radial velocity can be written as

$$\begin{aligned} \varphi_{0,r}^+(a/H^+, z, t) &\approx t \left( \sum_{n=0}^{140} c_n \sigma_n \frac{K_0'(\sigma_n \frac{a}{H^+})}{K_0(\sigma_n \frac{a}{H^+})} \cos(\sigma_n z) + \sum_{n=141}^{1999} c_n \sigma_n \frac{K_0'(\sigma_n \frac{a}{H^+})}{K_0(\sigma_n \frac{a}{H^+})} \cos(\sigma_n z) \right) \\ &\approx -t \left( \sum_{n=0}^{140} c_n \sigma_n \frac{K_1(\sigma_n \frac{a}{H^+})}{K_0(\sigma_n \frac{a}{H^+})} \cos(\sigma_n z) + \sum_{n=141}^{1999} c_n \sigma_n \cos(\sigma_n z) \right). \end{aligned}$$

by using (A.2). In Fig. (3.6), the velocity is plotted for three different values  $a/H^+ = 0.5, 1, 1.5$ . Table 3.5 provides the numerical values of the radial velocities of the initially

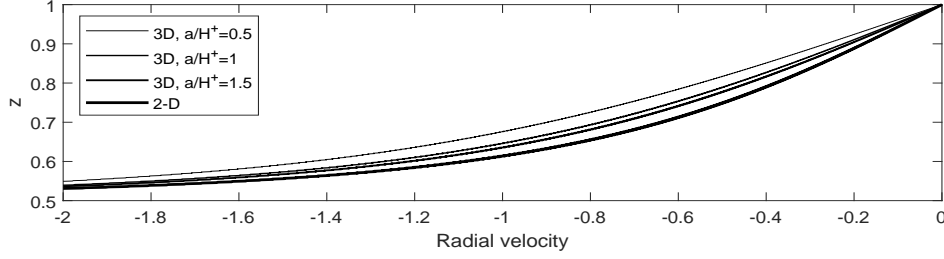


Figure 3.6. Radial velocity of the initially vertical free surface  $\varphi_{0,r}^+(a/H^+, z, t)$  for  $a/H^+ = 0.5, 1, 1.5$ . and 2-D

vertical free surface for  $a/H^+ = 0.5, 1, 1.5$  near  $z = \delta$ . Close to the bottom circle, the values increase rapidly towards the negative direction, demonstrating the singularity there. The radial velocities of the initially vertical free surface presented in Fig. 3.6 are same to the horizontal velocities of the initially vertical free surface of the liquid on the right, for  $\delta = 0.5$  and liquids having same density presented in Fig. 9 in Yilmaz et al. (2013a).

Table 3.5. Radial velocities of the initially vertical free surface near the bottom circle

$z$	$\varphi_{0,r}^+(0.5, z, t)$	$\varphi_{0,r}^+(1, z, t)$	$\varphi_{0,r}^+(1.5, z, t)$
0.501	-8.236928559655034	-8.025861916453382	-7.951427421424839
0.502	-6.111019944460889	-5.900915084114108	-5.826441139355690
0.503	-5.591022229303540	-5.382585253260065	-5.308441310650255

The vertical velocity of the lower free surface can be expressed by the equation

$$\begin{aligned}
\varphi_{0,z}^-(r, \delta, t) &\approx t \left( \sum_{m=0}^{70} (-1)^{m+1} d_m \frac{\sigma_m}{\delta} \frac{I_0(\sigma_m \frac{r}{\delta})}{I_0(\sigma_m \frac{a/H^+}{\delta})} + \sum_{m=71}^{999} (-1)^{m+1} d_m \frac{\sigma_m}{\delta} \frac{I_0(\sigma_m \frac{r}{\delta})}{I_0(\sigma_m \frac{a/H^+}{\delta})} \right) \\
&\approx t \left( \sum_{m=0}^{70} (-1)^{m+1} d_m \frac{\sigma_m}{\delta} \frac{I_0(\sigma_m \frac{r}{\delta})}{I_0(\sigma_m \frac{a/H^+}{\delta})} + \sqrt{\frac{a}{H^+ r}} \sum_{m=71}^{999} (-1)^{m+1} d_m \frac{\sigma_m}{\delta} e^{\sigma_m(r-a/H^+)/\delta} \right).
\end{aligned} \tag{3.75}$$

For  $a/H^+ = 0.5, 1, 1.5$  the vertical velocity is plotted in Figure 3.7. The velocities are shifted by  $a/H^+$  to the left in order to compare. Table 3.6 provides the numerical data

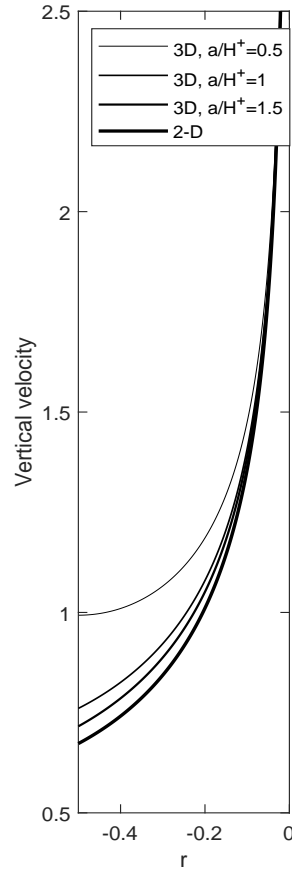


Figure 3.7. Vertical velocity of the lower free surface  $\varphi_{0,z}^-(r, \delta, t)$  for  $a/H^+ = 0.5, 1, 1.5$ . and 2-D

of the vertical velocities near  $r = a/H^+$ . Close to the bottom circle the values increase rapidly upwards, showing the presence of a singularity. We notice that the vertical velocity of the lower free surface presented in Fig. 3.7 is same to the vertical velocity of the free surface of the shallower liquid Fig. 8 in Yilmaz et al. (2013a), for the case  $\delta = 0.5$  and liquids having the same density.



Table 3.6. Vertical velocities of the lower free surface near the bottom circle

$r$	$\varphi_{0,z}^-(r, \delta, t)$ $a/H^+ = 0.5$	$\varphi_{0,z}^-(r, \delta, t)$ $a/H^+ = 1$	$\varphi_{0,z}^-(r, \delta, t)$ $a/H^+ = 1.5$
-0.003	5.115672631118379	5.108215900319818	5.105781594358199
-0.002	5.864411101265139	5.858691521687085	5.856818619791557
-0.001	7.209457356212002	7.205925364175235	7.204764499068431

### 3.6.4. Free surface shapes

We continue this section by providing the results of the numerical computations for the free surface shapes for  $\delta = 0.5$ , and  $a/H^+ = 0.5, 1, 1.5$ . First, we present the top free surface shape  $\eta_0(r, t)$  (see Fig. 3.8) for three different ratios  $a/H^+$ . In the graph, the top free surface shape from the 2-D problem is plotted too for comparison. Here the 3-D graphs are shifted by  $a/H^+$  to the left, due to the 2-D problem in Yilmaz et al. (2013a) having the flat sheet separation in  $x = 0$ , and the 3-D problem having the cylindrical cavity in  $r = a/H^+$ . By increasing the ratio  $a/H^+$  the top free surface shape approaches to the 2-D problem top free surface shape. For  $n > 145$ , in the summation, we use (A.2), the asymptotic expansion for large arguments of the modified Bessel function,

$$\begin{aligned} \eta_0(r, t) &\approx \frac{t^2}{2} \left( \sum_{n=0}^{145} (-1)^n c_n \sigma_n \frac{K_0(\sigma_n r)}{K_0(\sigma_n \frac{a}{H^+})} + \sum_{n=146}^{1999} (-1)^n c_n \sigma_n \frac{K_0(\sigma_n r)}{K_0(\sigma_n \frac{a}{H^+})} \right) \\ &\approx \frac{t^2}{2} \left( \sum_{n=0}^{145} (-1)^n c_n \sigma_n \frac{K_0(\sigma_n r)}{K_0(\sigma_n \frac{a}{H^+})} + \sqrt{\frac{a}{H^+ r}} \sum_{n=146}^{1999} (-1)^n c_n \sigma_n e^{-\sigma_n (r-a/H^+)} \right). \end{aligned}$$

The vertical free surface  $\zeta_0(z, t)$  is plotted in Fig. 3.9 for three different values  $a/H^+$ . For comparison, the 2D initially vertical free surface of the liquid on the right for  $\delta = 0.5$  and  $\gamma = 1$  is plotted too. An increase in  $a/H^+$ , shows that the vertical free surface of the 3-D problem approaches the vertical free surface of the 2-D problem. In the summation, for  $n > 140$ , the ratio of the modified Bessel functions of second kind is

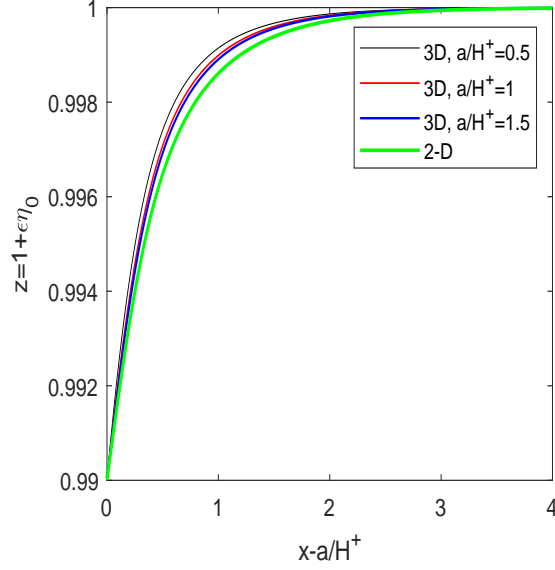


Figure 3.8. Top free surface shape of the 2-D and 3-D case for different ratios  $a/H^+ = 0.5, 1, 1.5$  and for  $\delta = 0.5, \varepsilon = 0.01$

replaced by (A.2), the asymptotic expansions for large arguments

$$\begin{aligned} \zeta_0(z, t) &\approx \frac{t^2}{2} \left( \sum_{n=0}^{140} c_n \sigma_n \frac{K_0'(\sigma_n \frac{a}{H^+})}{K_0(\sigma_n \frac{a}{H^+})} \cos(\sigma_n z) + \sum_{n=141}^{1999} c_n \sigma_n \frac{K_0'(\sigma_n \frac{a}{H^+})}{K_0(\sigma_n \frac{a}{H^+})} \cos(\sigma_n z) \right) \\ &\approx \frac{-t^2}{2} \left( \sum_{n=0}^{140} c_n \sigma_n \frac{K_1(\sigma_n \frac{a}{H^+})}{K_0(\sigma_n \frac{a}{H^+})} \cos(\sigma_n z) + \sum_{n=141}^{1999} c_n \sigma_n \cos(\sigma_n z) \right). \end{aligned}$$

The lower free surface  $v_0(r, t)$  for three different values  $a/H^+$  is provided in Fig. 3.10. For comparison, the 2-D free surface of the liquid on the left for  $\delta = 0.5$  and  $\gamma = 1$ , is provided too. Here the 3-D graphs are shifted by  $a/H^+$  to the left, in order to compare with the 2-D graph. An increase in  $a/H^+$  shows that the lower free surface of the 3-D problem approaches the lower free surface of the 2-D problem. In the computations, for  $m > 70$ , we replace the modified Bessel functions using (A.1), and the equation of the

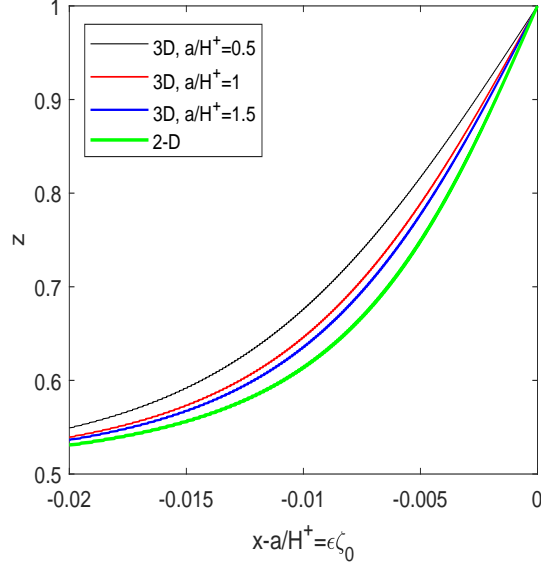


Figure 3.9. Vertical free surface shape for  $\delta = 0.5$  and  $\varepsilon = 0.01$  computed for the 2-D case and for the 3-D case for different ratios  $a/H^+ = 0.5, 1, 1.5$

lower free surface becomes

$$\begin{aligned}
 v_0(r, t) &\approx \frac{t^2}{2} \left( \sum_{m=0}^{70} (-1)^{m+1} d_m \frac{\sigma_m}{\delta} \frac{I_0(\sigma_m \frac{r}{\delta})}{I_0(\sigma_m \frac{a/H^+}{\delta})} + \sum_{m=71}^{999} (-1)^{m+1} d_m \frac{\sigma_m}{\delta} \frac{I_0(\sigma_m \frac{r}{\delta})}{I_0(\sigma_m \frac{a/H^+}{\delta})} \right) \\
 &\approx \frac{t^2}{2} \left( \sum_{m=0}^{70} (-1)^{m+1} d_m \frac{\sigma_m}{\delta} \frac{I_0(\sigma_m \frac{r}{\delta})}{I_0(\sigma_m \frac{a/H^+}{\delta})} + \sqrt{\frac{a}{H^+ r}} \sum_{m=71}^{999} (-1)^{m+1} d_m \frac{\sigma_m}{\delta} e^{\sigma_m (r-a/H^+)/\delta} \right).
 \end{aligned} \tag{3.76}$$

To conclude, the radial and vertical velocities at the interface match well at  $r = a/H, z = 0$ , but we do not have a good match at  $r = a/H, z = \delta$ , where the singularities are observed. The radial velocity of the initial vertical free surface deflects to the negative direction as we approach  $z = \delta$ , and on the other side, the vertical velocity of the lower free surface deflects to the negative direction too as we approach the lower circle of the cavity. The initial vertical free surface shape deflects to the left near  $r = a/H, z = -1$ , because of the presence of the singularities there. The lower free surface shape deflects upwards near the lower circle, indicating a jet formation at this circle. These results coincide with the ones found by Yilmaz et al. (2013a) for the 2-D case. Furthermore, in the analysis at

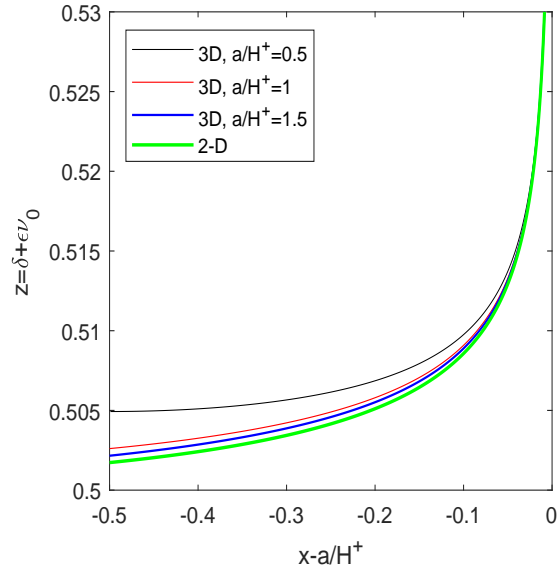


Figure 3.10. Lower free surface shape  $v_0$  for  $\delta = 0.5$  and  $\epsilon = 0.01$  computed for the 2-D case and for the 3-D case for different ratios  $a/H^+ = 0.5, 1, 1.5$

the bottom circle in Sec. 3.4, we find out that not only the singularities are conserved, but also the type of singularities at the lower circle is power singularity  $r^{-1/3}$ , same to the one at the triple point in the 2-D case. Finally, the free surface shapes, by sending the centre of cavity and the radius to infinity and keeping their distance constant, converge to the free surface shapes of the 2-D dam break problem of two immiscible fluids.

## CHAPTER 4

### THE GRAVITY DRIVEN FREE SURFACE FLOW CAUSED BY THE COLLAPSE OF A RECTANGULAR SECTION OF A VERTICAL PLATE

Three-dimensional problem of gravity-driven flow caused by the collapse of a rectangular section of a vertical plate located in front of a liquid region is investigated. Before the collapse, the fluid region  $\Omega'(0)$  is  $x' > 0$ ,  $-\infty < y' < \infty$ ,  $-H < z' \leq 0$ , and the vertical plate is positioned at  $x' = 0$ ,  $-\infty < y' < \infty$ ,  $-H < z' \leq 0$ . Here the prime stands for the dimensional variables and  $H$  represents the liquid depth (see Fig.4.1). Initially, the region  $x' > 0$ ,  $-\infty < y' < \infty$ ,  $z' = 0$  represents the top free surface.

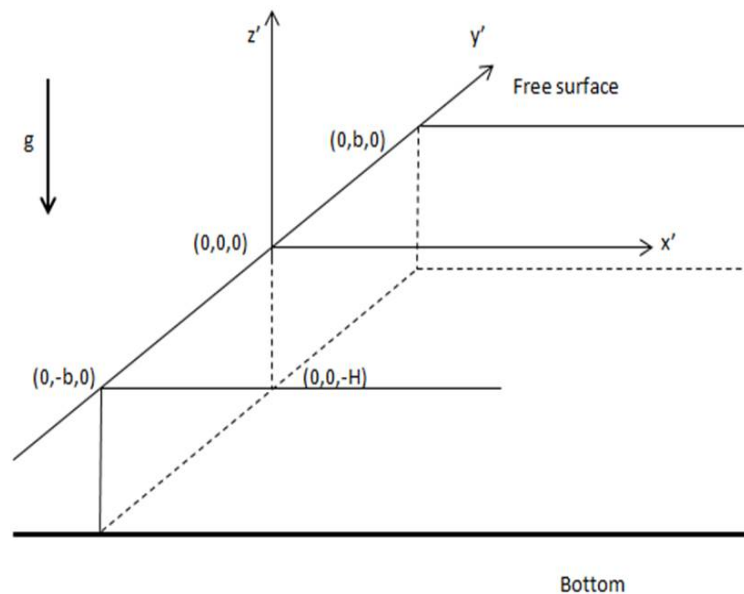


Figure 4.1. Flow region at initial time  $t' = 0$

At time  $t' = 0$ , a rectangular section  $x' = 0$ ,  $-b \leq y' \leq b$ ,  $-H < z' \leq 0$  of the vertical plate collapses, causing the start of a gravity-driven flow. For small times, the flow is assumed to be potential and three-dimensional. Immediately after the collapse of the

rectangular section, a vertical free surface shape is formed at  $x' = 0$ ,  $-b \leq y' \leq b$ ,  $-H < z' < 0$ , which under the gravity force starts deforming. Attention is paid in determining the shape of the vertical free surface. Besides, it is of interest checking the behaviour of the velocity field at three of the edges of the rectangular section, the right edge  $x' = 0$ ,  $y' = -b$ ,  $-H < z' \leq 0$ , the left edge  $x' = 0$ ,  $y' = b$ ,  $-H < z' \leq 0$ , and the bottom edge  $x' = 0$ ,  $-b \leq y' \leq b$ ,  $z' = -H$ .

Fourier series method and BEM is used in the solution of the problem. The velocity field is expected to be singular at the bottom edge, because of a mismatch of the boundary conditions along this line. The horizontal velocity of the initially vertical free surface at  $x' = 0$ ,  $y' = 0$  and  $-H < z' \leq 0$ , is expected to be similar to the horizontal velocity of the initially vertical free surface in the 2-D dam break problem by Korobkin and Yilmaz (2009).

#### 4.1. Formulation of the problem

The fluid is considered to be irrotational, implying the existence of a velocity potential  $\varphi'(x', y', z', t')$ . It is assumed too that the fluid is incompressible, therefore the velocity potential satisfies the Laplace's equation:

$$\nabla^2 \varphi' = 0 \quad (\text{in } \Omega'(t')). \quad (4.1)$$

Here  $\Omega'(t')$ , denotes the flow region. At the initial time,  $t' = 0$ , when the rectangular section collapses, a vertical free surface forms at its place. Both free surfaces, the top free surface and the rectangular one, under the gravitational force, will change their shape. The conditions on these free surfaces are described below. The first condition, is that the particles on the free surface remain on the free surface. So, the kinematic conditions are:

$$\varphi'_{z'} = \varphi'_{x'} \eta'_{x'} + \varphi'_{y'} \eta'_{y'} + \eta'_{t'} \quad (\text{on } TS'(t')), \quad (4.2)$$

$$\varphi'_{x'} = \varphi'_{y'} h'_{y'} + \varphi'_{z'} h'_{z'} + h'_{t'} \quad (\text{on } RS'(t')), \quad (4.3)$$

where  $TS(t')$  is the top free surface of the region:  $x' > 0$ ,  $-\infty < y' < \infty$ ,  $z' = \eta'(x', y', t')$  and  $RS(t')$  is the rectangular free surface:  $x' = h'(y', z', t')$ ,  $-b \leq y' \leq b$ ,  $-H < z' < \eta'(0, y', t')$ . Here  $\eta'(x', y', t')$  and  $h'(y', z', t')$  stand for the shapes of the top free surface and rectangular free surface respectively, and have to be determined.

The next condition on the free surface is that, for inviscid fluids, the pressure is equal to the atmospheric pressure, therefore the Bernoulli's equation for unsteady irrotational flow

$$\varphi'_t + \frac{1}{2} |\nabla \varphi'|^2 + gz' = -\frac{P}{\rho_0} \quad (\text{on } \Omega'(t')), \quad (4.4)$$

is

$$\varphi'_t + \frac{1}{2} |\nabla \varphi'|^2 + gz' = 0 \quad (\text{on } FS'(t')), \quad (4.5)$$

where  $FS'(t') = TS'(t') \cup RS'(t')$ .

The other BC's are imposed on the rigid bottom and the rigid vertical plate, which is the part of the vertical plate that does not collapse. There is no horizontal velocity component on the rigid vertical plate

$$\varphi'_{x'} = 0 \quad (\text{on } VS'(t')), \quad (4.6)$$

and no vertical velocity component on the rigid bottom

$$\varphi'_{z'} = 0 \quad (\text{on } BS'(t')), \quad (4.7)$$

where  $VS(t')$  and  $BS(t')$  represent the rigid vertical plate surface  $x' = 0$ ,  $-\infty < y' < -b \cup b < y' < \infty$ ,  $-H < z' \leq 0$  and the rigid bottom surface  $z' = -H$  respectively.

Initially there is no velocity potential, and the free surfaces are at their starting positions

$$\varphi'(x', y', z', 0) = 0, \quad \eta'(x', y', 0) = 0, \quad h'(y', z', 0) = 0, \quad (4.8)$$

and there is no flow far from the centre

$$\varphi' \rightarrow 0 \quad (\sqrt{x'^2 + y'^2} \rightarrow +\infty). \quad (4.9)$$

We present the following non-dimensional variables

$$\begin{aligned}
x' &= xH, & y' &= yH, & z' &= zH, & t' &= Tt, \\
\varphi' &= gHT\varphi, & p' &= \rho_0gHp, & T &= \varepsilon^{1/2}\sqrt{H/g} \\
\eta' &= S_1\eta, & h' &= S_2h, \\
S_1/H &= O(\varepsilon), & S_2/H &= O(\varepsilon).
\end{aligned} \tag{4.10}$$

and write the new dimensionless equations by replacing (4.10) in the boundary value problem (4.1)-(4.9). The nondimensional potential  $\varphi(x, y, z, t)$  satisfies the following equations:

$$\nabla^2\varphi = 0 \quad (\text{in } \Omega(t)), \tag{4.11}$$

$$\varphi_z = \varepsilon\varphi_x\eta_x + \varepsilon\varphi_y\eta_y + \eta_t \quad (\text{on } TS(t)), \tag{4.12}$$

$$\varphi_x = \varepsilon\varphi_y h_y + \varepsilon\varphi_z h_z + h_t \quad (\text{on } RS(t)), \tag{4.13}$$

$$-p = \varphi_t + \frac{1}{2}\varepsilon|\nabla\varphi|^2 + z \quad (\text{in } \Omega(t)), \tag{4.14}$$

$$p = p_0 = \varphi_t + \frac{1}{2}\varepsilon|\nabla\varphi|^2 + z = 0 \quad (\text{on } FS(t)), \tag{4.15}$$

$$\varphi_x = 0 \quad (\text{on } VS(t)), \tag{4.16}$$

$$\varphi_z = 0 \quad (\text{on } BS(t)), \tag{4.17}$$

$$\varphi(x, y, z, 0) = 0, \quad \eta(x, y, 0) = 0, \quad h(y, z, 0) = 0, \quad (t = 0) \tag{4.18}$$

$$\varphi \rightarrow 0 \quad (\sqrt{x^2 + y^2} \rightarrow +\infty). \tag{4.19}$$

Here  $\Omega(t)$  is the flow region,  $FS(t) = TS(t) \cup RS(t)$  is the free surface of the region, where  $TS(t)$  is the top free surface of the region:  $x > 0$ ,  $-\infty < y < \infty$ ,  $z = \varepsilon\eta(x, y, t, \varepsilon)$  and  $RS(t)$  is the rectangular free surface:  $x = \varepsilon h(y, z, t, \varepsilon)$ ,  $-b/H \leq y \leq b/H$ ,  $-1 < z < \varepsilon\eta(0, y, t, \varepsilon)$ .  $VS(t)$  and  $BS(t)$  represent the rigid vertical surface:  $x = 0$ ,  $-\infty < y < -b/H \cup b/H < y < \infty$ ,  $-1 < z < 0$  and the rigid bottom surface  $z = -1$  respectively.



We search for a solution of the BVP (4.11)-(4.19), as  $\varepsilon \rightarrow 0$  in the form

$$\begin{aligned}\varphi(x, y, z, t, \varepsilon) &= \varphi_0(x, y, z, t) + \varepsilon\varphi_1(x, y, z, t) + \mathcal{O}(\varepsilon^2), \\ \eta(x, y, t, \varepsilon) &= \eta_0(x, y, t) + \varepsilon\eta_1(x, y, t) + \mathcal{O}(\varepsilon^2), \\ h(y, z, t, \varepsilon) &= h_0(y, z, t) + \varepsilon h_1(y, z, t) + \mathcal{O}(\varepsilon^2).\end{aligned}\tag{4.20}$$

## 4.2. Leading-order outer problem and solution by boundary element method

Substituting the asymptotic expansions (4.20) in the BVP (4.11)-(4.19), as  $\varepsilon \rightarrow 0$  we get the boundary-value problem for the leading-order velocity potential. The Laplace's equation (4.11) becomes

$$\nabla^2\varphi_0 = 0 \quad (x > 0, -\infty < y < \infty, -1 < z < 0).\tag{4.21}$$

The dynamic boundary condition (4.15) and the kinematic condition (4.12) on the top free surface become

$$\varphi_0 = 0, \quad \frac{\partial\eta_0}{\partial t} = \frac{\partial\varphi_0}{\partial z} \quad (x > 0, -\infty < y < \infty, z = 0).\tag{4.22}$$

The dynamic boundary condition (4.15) and the kinematic condition (4.13) on the rectangular free surface give

$$\varphi_0 = -zt, \quad \frac{\partial h_0}{\partial t} = \frac{\partial\varphi_0}{\partial x} \quad (x = 0, |y| \leq b/H, -1 < z < 0).\tag{4.23}$$

The boundary condition on the rigid vertical surface (4.16) gives

$$\frac{\partial\varphi_0}{\partial x} = 0 \quad (x = 0, |y| > b/H, -1 < z < 0),\tag{4.24}$$

and the boundary condition on the rigid bottom (4.17) gives

$$\frac{\partial \varphi_0}{\partial z} = 0 \quad (x > 0, -\infty < y < \infty, z = -1). \quad (4.25)$$

The initial conditions (4.18) yield

$$\varphi_0(x, y, z, 0) = 0, \quad \eta_0(x, y, 0) = 0, \quad h_0(y, z, t) = 0, \quad (t = 0). \quad (4.26)$$

The condition at the far field (4.19) becomes

$$\varphi_0 \rightarrow 0 \quad (\sqrt{x^2 + y^2} \rightarrow \infty). \quad (4.27)$$

The intersection of the rectangular section and the rigid bottom is the line  $x = 0, -b/H \leq y \leq b/H, z = -1$ . The vertical velocities along this line should be the same. From (4.23) we get  $\varphi_{0,z} = -t$ , from (4.25) we have  $\varphi_{0,z} = 0$ , which do not coincide. Singularity within the mathematical model (4.21)-(4.27) is expected at the line  $x = 0, -b/H \leq y \leq b/H, z = -1$ .

The solution method will follow partly the one in Renzi and Dias (2013). Separating the  $z$  dependence, the solution to (4.21)-(4.27) can be written as

$$\varphi_0(x, y, z, t) = t \sum_{n=0}^{\infty} \varphi_{0n}(x, y) \sin(\sigma_n z), \quad (4.28)$$

where  $\sigma_n = \frac{\pi/2}{2n+1}$ . Equation (4.28) satisfies the Laplace's equation (4.21), the dynamic boundary condition on the upper free surface (4.22), the kinematic condition on the horizontal bottom (4.25) and the initial condition (4.26). Replacing (4.28) in (4.21) and using the orthogonality relation of the sine function

$$\int_{-1}^0 \sin(\sigma_n z) \sin(\sigma_m z) dz = \frac{1}{2} \delta_{nm}, \quad n, m = 0, 1, \dots,$$

where  $\delta_{nm}$  is the Kronecker symbol, we derive the modified Helmholtz equation

$$\nabla^2 \varphi_{0n} - \sigma_n^2 \varphi_{0n} = 0 \quad (x > 0, -\infty < y < \infty, -1 < z < 0), \quad (4.29)$$

with the boundary conditions (4.23), (4.24) and (4.27) being transformed to

$$\varphi_{0n}(0, y) = \frac{2(-1)^{n+1}}{\sigma_n^2} \quad (x = 0, |y| \leq b/H, -1 < z < 0), \quad (4.30)$$

$$\frac{\partial}{\partial x} \varphi_{0n}(0, y) = 0 \quad (x = 0, |y| > b/H, -1 < z < 0), \quad (4.31)$$

$$\varphi_{0n}(x, y) \rightarrow 0 \quad (\sqrt{x^2 + y^2} \rightarrow \infty), \quad (4.32)$$

respectively (See Fig. 4.2). So we have a boundary value problem on the right half plane of  $xy$ -plane.

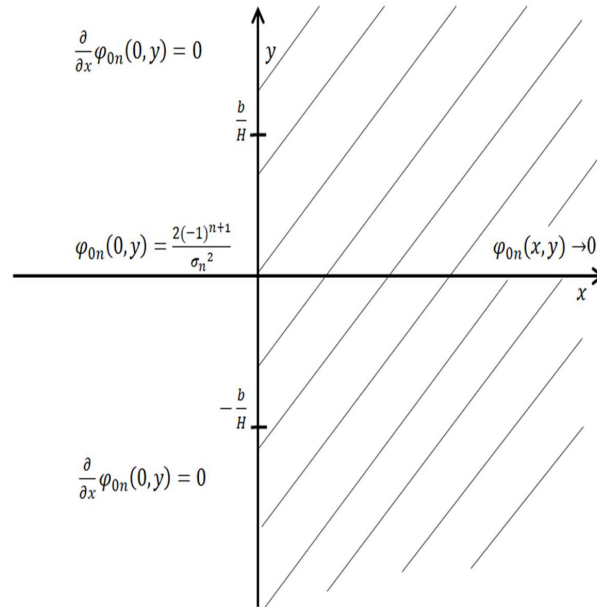


Figure 4.2. BVP for  $\varphi_{0n}$

The Green's function  $G(\mathbf{x}, \mathbf{x}_0)$  is used in order to solve the boundary value problem (4.29)-(4.32), i.e,

$$\nabla^2 G - \sigma_n^2 G = -\delta(\mathbf{x} - \mathbf{x}_0), \quad (4.33)$$

with homogeneous boundary conditions

$$G(0, y; x_0, y_0) = 0 \quad (x = 0, |y| \leq b/H, -1 < z < 0), \quad (4.34)$$

$$\frac{\partial}{\partial x} G(0, y; x_0, y_0) = 0 \quad (x = 0, |y| > b/H, -1 < z < 0), \quad (4.35)$$

$$G(x, y; x_0, y_0) \rightarrow 0 \quad (\sqrt{x^2 + y^2} \rightarrow \infty), \quad (4.36)$$

where the notation  $G(\mathbf{x}, \mathbf{x}_0) = G(x, y; x_0, y_0)$  represents the response at  $\mathbf{x}$  due to a source at  $\mathbf{x}_0$  and  $\delta(\mathbf{x} - \mathbf{x}_0)$  represents the two-dimensional Dirac delta function (Appendix B).

The solutions of the modified Helmholtz equation symmetric around  $R = 0$  are the solutions of

$$\frac{1}{R} \frac{d}{dR} \left( R \frac{dG}{dR} \right) - \sigma_n^2 G = 0, \quad (4.37)$$

which can be transformed to the modified Bessel equation

$$\bar{R}^2 \frac{d^2 G}{d\bar{R}^2} + \bar{R} \frac{dG}{d\bar{R}} - \bar{R}^2 G = 0, \quad (4.38)$$

where  $R = |\mathbf{x} - \mathbf{x}_0|$  and  $\bar{R} = \sigma_n R$ . The solutions to (4.38) are the linear combinations of the modified Bessel functions of the first and second kind of order zero

$$G(\bar{R}) = c_1 I_0(\bar{R}) + c_2 K_0(\bar{R}),$$

which should tend to zero for large arguments, therefore  $c_1 = 0$  and

$$G(\sigma_n R) = c_2 K_0(\sigma_n R).$$

In order to calculate the coefficient  $c_2$ , we replace the  $k$  in C.1 by  $\pm i\sigma_n$  and divide C.2 by  $4\pi$  (see Appendix C) and get

$$c_2 K_0(\sigma_n R) = \frac{i}{4} H_0^{(1)}(\pm i\sigma_n R), \quad (4.39)$$

where  $H_n^{(1)}$  is the Hankel function of the first kind of order  $n$  and  $i$  is the imaginary unit. Replacing the relation

$$K_n(x) = \frac{1}{2}\pi i^{n+1} H_n^{(1)}(ix)$$

on left side of (4.39), yields the coefficient  $c_2 = \frac{1}{2\pi}$ . Therefore, the solution to (4.37), which is the infinite domain Green's function, is

$$G(\sigma_n R) = \frac{1}{2\pi} K_0(\sigma_n R), \quad (4.40)$$

which satisfies the radiation condition (4.36). However it is difficult to satisfy the boundary conditions (4.34) and (4.35) simultaneously. Instead we shall use two different integral equations. In one of them  $G_1(\mathbf{x}, \mathbf{x}_0) = 0$  on  $y$ -axis, in the other  $\frac{\partial}{\partial x} G_2(\mathbf{x}, \mathbf{x}_0) = 0$  on  $y$ -axis. Using the method of images we achieve below the required Green's functions at  $x = 0$ .

1. First problem:  $G_1(0, y; x_0, y_0) = 0$

To obtain a solution that is zero at  $x = 0$ , it is required to place a negative image source  $-\delta(\mathbf{x} - \mathbf{x}_0^*)$  at  $\mathbf{x} = \mathbf{x}_0^*$  to the source  $\delta(\mathbf{x} - \mathbf{x}_0)$  at  $\mathbf{x} = \mathbf{x}_0$ , where

$$\begin{aligned} \mathbf{x}_0 &= x_0 \hat{\mathbf{i}} + y_0 \hat{\mathbf{j}} \\ \mathbf{x}_0^* &= -x_0 \hat{\mathbf{i}} + y_0 \hat{\mathbf{j}}. \end{aligned}$$

Therefore the Green's function is

$$G_1 = \frac{1}{2\pi} K_0(\sigma_n | \mathbf{x} - \mathbf{x}_0 |) - \frac{1}{2\pi} K_0(\sigma_n | \mathbf{x} - \mathbf{x}_0^* |). \quad (4.41)$$

2. Second problem:  $\frac{\partial}{\partial x} G_2(0, y; x_0, y_0) = 0$

Here, as we are dealing with the derivative, plotting a positive image source  $\delta(\mathbf{x} - \mathbf{x}_0^*)$  at  $\mathbf{x} = \mathbf{x}_0^*$  will give zero at  $x = 0$ , thus the Green's function is

$$G_2 = \frac{1}{2\pi} K_0(\sigma_n | \mathbf{x} - \mathbf{x}_0 |) + \frac{1}{2\pi} K_0(\sigma_n | \mathbf{x} - \mathbf{x}_0^* |). \quad (4.42)$$

To obtain the solution of (4.29)-(4.32) using the Green's function, we can utilize the Green's formula

$$\iint_D (f\nabla^2 g - g\nabla^2 f) dA = \oint_C (f\nabla g - g\nabla f) \cdot \hat{\mathbf{n}} dS \quad (4.43)$$

for  $f = \varphi_{0n}(\mathbf{x})$  and  $g = G(\mathbf{x}, \mathbf{x}_0)$ . Using equations (4.29) and (4.33) on the left of (4.43) and considering a large semicircle (see Fig. 4.2), whose radius tends to infinity for the right hand side of (4.43), we obtain,

$$- \iint_D \varphi_{0n}(\mathbf{x}) \delta(\mathbf{x} - \mathbf{x}_0) dA = \int_{-\infty}^{\infty} \left( \varphi_{0n}(\mathbf{x}) \frac{\partial}{\partial x} G(\mathbf{x}, \mathbf{x}_0) - G(\mathbf{x}, \mathbf{x}_0) \frac{\partial}{\partial x} \varphi_{0n}(\mathbf{x}) \right) \Big|_{x=0} dy. \quad (4.44)$$

By the fundamental operator property of the two-dimensional Dirac delta function (B.1), (4.44) becomes

$$\frac{1}{2} \varphi_{0n}(\mathbf{x}_0) = \int_{-\infty}^{\infty} \left( \varphi_{0n}(\mathbf{x}) \frac{\partial}{\partial x} G(\mathbf{x}, \mathbf{x}_0) - G(\mathbf{x}, \mathbf{x}_0) \frac{\partial}{\partial x} \varphi_{0n}(\mathbf{x}) \right) \Big|_{x=0} dy. \quad (4.45)$$

In order to solve (4.45), we have two options, either  $G = 0$  or  $\partial G / \partial x = 0$ . Next, we treat these cases separately.

#### 4.2.1. First problem: The Green's function is zero at $x = 0$

Since  $G_1 = 0$  at  $x = 0$ , (4.45) reduces to

$$\frac{1}{2} \varphi_{0n}(\mathbf{x}_0) = \int_{-\infty}^{\infty} \varphi_{0n}(\mathbf{x}) \frac{\partial}{\partial x} G_1(\mathbf{x}, \mathbf{x}_0) \Big|_{x=0} dy,$$

which by (4.30) gives

$$\begin{aligned} \frac{1}{2}\varphi_{0n}(\mathbf{x}_0) &= \int_{-\infty}^{-b/H} \varphi_{0n}(\mathbf{x}) \frac{\partial}{\partial x} G_1(\mathbf{x}, \mathbf{x}_0) \Big|_{x=0} dy + \frac{2(-1)^{n+1}}{\sigma_n^2} \int_{-b/H}^{b/H} \frac{\partial}{\partial x} G_1(\mathbf{x}, \mathbf{x}_0) \Big|_{x=0} dy \\ &+ \int_{b/H}^{\infty} \varphi_{0n}(\mathbf{x}) \frac{\partial}{\partial x} G_1(\mathbf{x}, \mathbf{x}_0) \Big|_{x=0} dy. \end{aligned} \quad (4.46)$$

The problem is symmetric with respect to the line  $y = 0$ , therefore

$$\varphi_{0n}(x, y) = \varphi_{0n}(x, -y),$$

and (4.46) can be arranged as

$$\begin{aligned} -\frac{1}{2}\varphi_{0n}(\mathbf{x}_0) + \int_{b/H}^{\infty} \varphi_{0n}(\mathbf{x}) \left( \frac{\partial}{\partial x} G_1(x, y; x_0, y_0) + \frac{\partial}{\partial x} G_1(x, -y; x_0, y_0) \right) \Big|_{x=0} dy \\ = \frac{2(-1)^n}{\sigma_n^2} \int_{-b/H}^{b/H} \frac{\partial}{\partial x} G_1(\mathbf{x}, \mathbf{x}_0) \Big|_{x=0} dy. \end{aligned} \quad (4.47)$$

By reversing the roles of  $\mathbf{x}_0$  and  $\mathbf{x}$  and the Green's function's symmetry property

$$G(\mathbf{x}, \mathbf{x}_0) = G(\mathbf{x}_0, \mathbf{x}), \quad (4.48)$$

(4.47) becomes

$$\begin{aligned} -\frac{1}{2}\varphi_{0n}(\mathbf{x}) + \int_{b/H}^{\infty} \varphi_{0n}(\mathbf{x}_0) \left( \frac{\partial}{\partial x_0} G_1(x, y; x_0, y_0) + \frac{\partial}{\partial x_0} G_1(x, y; x_0, -y_0) \right) \Big|_{x_0=0} dy_0 \\ = \frac{2(-1)^n}{\sigma_n^2} \int_{-b/H}^{b/H} \frac{\partial}{\partial x_0} G_1(\mathbf{x}, \mathbf{x}_0) \Big|_{x_0=0} dy_0. \end{aligned} \quad (4.49)$$

By (4.41)

$$\frac{\partial}{\partial x_0} G_1(x, y, x_0, y_0) \Big|_{x_0=0} = \frac{1}{2\pi} x \sigma_n \frac{K_1(\sigma_n \sqrt{x^2 + (y - y_0)^2})}{\sqrt{x^2 + (y - y_0)^2}}, \quad (4.50)$$

and

$$\frac{\partial}{\partial x_0} G_1(x, y, x_0, -y_0) \Big|_{x_0=0} = \frac{1}{2\pi} x \sigma_n \frac{K_1(\sigma_n \sqrt{x^2 + (y + y_0)^2})}{\sqrt{x^2 + (y + y_0)^2}}, \quad (4.51)$$

which by being replaced in (4.49) give the first integral equation,

$$\begin{aligned} -\frac{1}{2}\varphi_{0n}(\mathbf{x}) + \frac{1}{\pi}x\sigma_n \int_{b/H}^{\infty} \varphi_{0n}(\mathbf{x}_0) \left( \frac{K_1(\sigma_n \sqrt{x^2 + (y - y_0)^2})}{\sqrt{x^2 + (y - y_0)^2}} + \frac{K_1(\sigma_n \sqrt{x^2 + (y + y_0)^2})}{\sqrt{x^2 + (y + y_0)^2}} \right) dy_0 \\ = \frac{2(-1)^n}{\sigma_n} \frac{1}{2\pi} x \int_{-b/H}^{b/H} \frac{K_1(\sigma_n \sqrt{x^2 + (y - y_0)^2})}{\sqrt{x^2 + (y - y_0)^2}} dy_0. \end{aligned} \quad (4.52)$$

The solution method follows the same technique used by Yilmaz et al. (2013a). The solution is achieved numerically by discretizing the boundary into small panels. It is assumed that the panels are straight line segments and the velocity potentials on these segments are constant. Therefore, (4.49) is discretised as

$$-\frac{1}{2}\varphi_{0n,i} + \sum_{j \in P} \varphi_{0n,j} \left( dg_{ij}^{(1)} + dg_{ij}^{(2)} \right) \Big|_{x_0=0} = \frac{2(-1)^n}{\sigma_n^2} \sum_{j \in Q} dg_{ij}^{(3)} \Big|_{x_0=0}, \quad \forall i \in P \cup Q \quad (4.53)$$

where  $\varphi_{0n,i}$  denotes the velocity potential on the  $i$ -th panel,  $P$  is the set of panels from  $[b/H, \infty)$ ,  $Q$  is the set of panels from  $[-b/H, b/H]$  and

$$\begin{aligned} dg_{ij}^{(1)} &= \int_{a_j-l}^{a_j+l} \frac{\partial}{\partial x_0} G_1(x_i, y_i; x_{0j}, y_{0j}) dy_{0j}, \\ dg_{ij}^{(2)} &= \int_{a_j-l}^{a_j+l} \frac{\partial}{\partial x_0} G_1(x_i, y_i; x_{0j}, -y_{0j}) dy_{0j}, \\ dg_{ij}^{(3)} &= \int_{a_j-l}^{a_j+l} \frac{\partial}{\partial x_0} G_1(x_i, y_i; x_{0j}, y_{0j}) dy_{0j}, \end{aligned}$$

where  $a_j$  denotes the middle point of the  $j$ -th panel with distance  $l$  from its endpoints.

Hence, for  $x_{0j} = 0$ ,

$$dg_{ij}^{(1)}(x_i, y_i, a_j) = \frac{1}{2\pi} x_i \sigma_n \int_{a_j-l}^{a_j+l} \left( \frac{K_1(\sigma_n \sqrt{x_i^2 + (y_i - y_{0j})^2})}{\sqrt{x_i^2 + (y_i - y_{0j})^2}} \right) dy_{0j}, \quad (4.54)$$

$$dg_{ij}^{(2)}(x_i, y_i, a_j) = \frac{1}{2\pi} x_i \sigma_n \int_{a_j-l}^{a_j+l} \left( \frac{K_1(\sigma_n \sqrt{x_i^2 + (y_i + y_{0j})^2})}{\sqrt{x_i^2 + (y_i + y_{0j})^2}} \right) dy_{0j}, \quad (4.55)$$



and

$$dg_{ij}^{(3)}(x_i, y_i, a_j) = \frac{1}{2\pi} x_i \sigma_n \int_{a_j-l}^{a_j+l} \left( \frac{K_1(\sigma_n \sqrt{x_i^2 + (y_i - y_{0j})^2})}{\sqrt{x_i^2 + (y_i - y_{0j})^2}} \right) dy_{0j}. \quad (4.56)$$

When  $i \neq j$  the integral in (4.54) presents no problem and is evaluated numerically (see Fig. 4.3). The expression inside the integral in (4.54) has a finite value multiplied by  $x_i = 0$ , therefore  $dg_{ij}^{(1)} = 0$ .

When  $i = j$  the integral in (4.54) should be treated carefully (see Fig. 4.4). The small

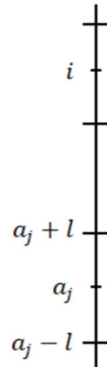


Figure 4.3. The element  $j$  does not coincide with element  $i$ .

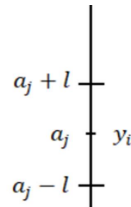


Figure 4.4. The element  $j$  coincides with element  $i$ ,  $a_j = (0, y_j)$ .

argument behaviour of the modified Bessel function of the second kind of order 1 (see A.6) is

$$K_1(z) \sim \frac{1}{z}. \quad (4.57)$$

Therefore  $dg_{ij}^{(1)}$  can be written as

$$\begin{aligned}
dg_{ij}^{(1)} &= \frac{\sigma_n}{2\pi} \int_{a_{j-l}}^{a_{j+l}} \left( \frac{x_i K_1(\sigma_n \sqrt{x_i^2 + (y_i - y_{0j})^2})}{\sqrt{x_i^2 + (y_i - y_{0j})^2}} - \frac{x_i}{\sigma_n(x_i^2 + (y_i - y_{0j})^2)} \right) dy_{0j} \\
&+ \frac{\sigma_n}{2\pi} \int_{a_{j-l}}^{a_{j+l}} \frac{x_i}{\sigma_n(x_i^2 + (y_i - y_{0j})^2)} dy_{0j}, \\
&= \frac{\sigma_n}{2\pi} \int_{a_{j-l}}^{a_{j+l}} \left( \frac{x_i K_1(\sigma_n \sqrt{x_i^2 + (y_i - y_{0j})^2})}{\sqrt{x_i^2 + (y_i - y_{0j})^2}} - \frac{x_i}{\sigma_n(x_i^2 + (y_i - y_{0j})^2)} \right) dy_{0j} \\
&- \frac{1}{2\pi} \arctan\left(\frac{y_i - y_{0j}}{x_i}\right) \Big|_{a_{j-l}}^{a_{j+l}},
\end{aligned}$$

or

$$dg_{ij}^{(1)} = \frac{\sigma_n}{2\pi} \int_{a_{j-l}}^{a_{j+l}} x_i f_1(x_i, y_i, y_{0j}) dy_{0j} - \frac{1}{2\pi} \arctan\left(\frac{y_i - y_{0j}}{x_i}\right) \Big|_{a_{j-l}}^{a_{j+l}}, \quad (4.58)$$

where

$$f_1(x_i, y_i, y_{0j}) = \begin{cases} 0 & y_i = y_{0j} \\ \frac{K_1(\sigma_n \sqrt{x_i^2 + (y_i - y_{0j})^2})}{\sqrt{x_i^2 + (y_i - y_{0j})^2}} - \frac{1}{\sigma_n(x_i^2 + (y_i - y_{0j})^2)} & \text{otherwise.} \end{cases}$$

For  $y_i = y_{0j}$  and  $x_i = 0$  we have  $f_1(x_i, y_i, y_{0j}) = 0$ , because of (4.57). For  $y_i \neq y_{0j}$ , and  $x_i = 0$ ,  $f_1(x_i, y_i, y_{0j})$  is finite. Therefore, for  $x_i = 0$  and any case of  $y_i$  and  $y_{0j}$ , the integral in (4.58) will be zero and consequently

$$dg_{ij}^{(1)} = -\frac{1}{2\pi} \left( \arctan\left(\frac{y_i - a_j - l}{x_i}\right) - \arctan\left(\frac{y_i - a_j + l}{x_i}\right) \right) = -\frac{1}{2\pi} \left( -\frac{\pi}{2} - \frac{\pi}{2} \right) = \frac{1}{2}.$$

for  $i = j$ , and 0 otherwise.

Concerning  $dg_{ij}^{(2)}$ , using the same line of reasoning as in  $dg_{ij}^{(1)}$ , we have

$$\begin{aligned}
dg_{ij}^{(2)} &= \frac{\sigma_n}{2\pi} \int_{a_j-l}^{a_j+l} \left( \frac{x_i K_1(\sigma_n \sqrt{x_i^2 + (y_i + y_{0j})^2})}{\sqrt{x_i^2 + (y_i + y_{0j})^2}} - \frac{x_i}{\sigma_n(x_i^2 + (y_i + y_{0j})^2)} \right) dy_{0j} \\
&+ \frac{\sigma_n}{2\pi} \int_{a_j-l}^{a_j+l} \frac{x_i}{\sigma_n(x_i^2 + (y_i + y_{0j})^2)} dy_{0j}, \\
&= \frac{\sigma_n}{2\pi} \int_{a_j-l}^{a_j+l} \left( \frac{x_i K_1(\sigma_n \sqrt{x_i^2 + (y_i + y_{0j})^2})}{\sqrt{x_i^2 + (y_i + y_{0j})^2}} - \frac{x_i}{\sigma_n(x_i^2 + (y_i + y_{0j})^2)} \right) dy_{0j} \\
&+ \frac{1}{2\pi} \arctan\left(\frac{y_i + y_{0j}}{x_i}\right) \Big|_{a_j-l}^{a_j+l},
\end{aligned}$$

or

$$dg_{ij}^{(2)} = \frac{\sigma_n}{2\pi} \int_{a_j-l}^{a_j+l} x_i f_2(x_i, y_i, y_{0j}) dy_{0j} + \frac{1}{2\pi} \arctan\left(\frac{y_i + y_{0j}}{x_i}\right) \Big|_{a_j-l}^{a_j+l}, \quad (4.59)$$

where

$$f_2(x_i, y_i, y_{0j}) = \begin{cases} 0 & y_i = y_{0j} \\ \frac{K_1(\sigma_n \sqrt{x_i^2 + (y_i + y_{0j})^2})}{\sqrt{x_i^2 + (y_i + y_{0j})^2}} - \frac{1}{\sigma_n(x_i^2 + (y_i + y_{0j})^2)} & \text{otherwise.} \end{cases}$$

Similar to the explanations used in calculating the integral in (4.58), the integral in (4.59) is zero too, therefore

$$dg_{ij}^{(2)} = \frac{1}{2\pi} \left( \arctan\left(\frac{y_i + a_j + l}{x_i}\right) - \arctan\left(\frac{y_i + a_j - l}{x_i}\right) \right) = \frac{1}{2\pi} \left( \frac{\pi}{2} - \frac{\pi}{2} \right) = 0, \quad (4.60)$$

for  $i = j$ , and 0 otherwise too, because the expression inside the integral in (4.55) has a finite value multiplied by  $x_i = 0$ .

$dg_{ij}^{(3)}$  is treated alike  $dg_{ij}^{(1)}$ , with the difference that the interval  $[a_j - l, a_j + l]$  is taken from  $[-b/H, b/H]$ , hence

$$dg_{ij}^{(3)} = -\frac{1}{2\pi} \left( \arctan\left(\frac{y_i - a_j - l}{x_i}\right) - \arctan\left(\frac{y_i - a_j + l}{x_i}\right) \right) = -\frac{1}{2\pi} \left( -\frac{\pi}{2} - \frac{\pi}{2} \right) = \frac{1}{2},$$

for  $i = j$ , and 0 otherwise, because of the multiplication of a finite value inside the integral

in (4.56) with  $x_i = 0$ .

Now that we have  $dg_{ij}^{(1)}$ ,  $dg_{ij}^{(2)}$ , and  $dg_{ij}^{(3)}$  values, replacing them in (4.53) yields a system of  $P + Q$  unknowns for each  $n = 0 : N$ ,

$$AX_n = B_n, \quad (4.61)$$

where the left part of (4.53) gives

$$A(i, j) = \begin{cases} -1/2 & i = j \leq Q \\ 0 & \text{otherwise,} \end{cases}$$

the unknowns are represented by

$$X_n(i, 1) = \varphi_{0n,i},$$

and the right side of (4.53) gives

$$B_n(i, 1) = \begin{cases} \frac{(-1)^n}{\sigma_n^2} & i \leq Q \\ 0 & \text{otherwise,} \end{cases}$$

where  $i = 1 : (P + Q)$ ,  $j = 1 : (P + Q)$ . By solving (4.61), we find that

$$\varphi_{0n,i} = \frac{2(-1)^{n+1}}{\sigma_n^2}, \quad i \leq Q, \quad (4.62)$$

coinciding with (4.30). Furthermore, replacing (4.62) in the derivative of (4.28) with respect to  $z$  and truncating the sum at  $n = 10000$ ,

$$\varphi_{0z,i}(x, y, z, t) = t \sum_{n=0}^{10000} \varphi_{0n,i}(x, y) \sigma_n \cos(\sigma_n z),$$

yields

$$\varphi_{0z,i} = -1 \quad i \leq Q,$$

with an error  $10^{-4}$ , coinciding with the derivative with respect to  $z$  of the boundary condition (4.23)

$$\varphi_{0z,i} = -t \quad (x = 0, |y| \leq b/H, -1 < z < 0),$$

for  $t = 1$ .

To conclude, by solving the first problem where the Green's function is 0 at  $x = 0$ , we show the validity of the boundary value problems (4.29)-(4.32) and (4.33)-(4.36).

#### 4.2.2. Second problem: The derivative of the Green's function is zero at $x = 0$

Since  $\frac{\partial}{\partial x} G_2 = 0$  at  $x = 0$ , (4.45) reduces to

$$-\frac{1}{2}\varphi_{0n}(\mathbf{x}_0) = \int_{-\infty}^{\infty} G_2(\mathbf{x}, \mathbf{x}_0) \frac{\partial}{\partial x} \varphi_{0n}(\mathbf{x}) \Big|_{x=0} dy,$$

which by (4.31) gives

$$-\frac{1}{2}\varphi_{0n}(\mathbf{x}_0) = \int_{-b/H}^{b/H} G_2(\mathbf{x}, \mathbf{x}_0) \frac{\partial}{\partial x} \varphi_{0n}(\mathbf{x}) \Big|_{x=0} dy. \quad (4.63)$$

Again by reversing  $\mathbf{x}_0$  and  $\mathbf{x}$  and using the symmetry property of the Green's function (4.48), equation (4.63) becomes

$$-\frac{1}{2}\varphi_{0n}(\mathbf{x}) = \int_{-b/H}^{b/H} G_2(\mathbf{x}, \mathbf{x}_0) \frac{\partial}{\partial x_0} \varphi_{0n}(\mathbf{x}_0) \Big|_{x_0=0} dy_0. \quad (4.64)$$

By (4.42)

$$G_2(\mathbf{x}, \mathbf{x}_0) \Big|_{x_0=0} = \frac{1}{\pi} K_0(\sigma_n \sqrt{x^2 + (y - y_0)^2}), \quad (4.65)$$

and by replacing (4.65) in (4.64) gives the second integral equation

$$-\frac{1}{2}\varphi_{0n}(\mathbf{x}) = \frac{1}{\pi} \int_{-b/H}^{b/H} K_0(\sigma_n \sqrt{x^2 + (y - y_0)^2}) \frac{\partial}{\partial x_0} \varphi_{0n}(\mathbf{x}_0) \Big|_{x_0=0} dy_0. \quad (4.66)$$

Notice that if  $y$  is restricted between  $-b/H$  and  $b/H$ , the right hand side of (4.66) is known from (4.30) and equation (4.66) becomes a Fredholm integral equation of the first kind in the unknown function  $\frac{\partial}{\partial x_0} \varphi_{0n}$ . For the numerical solution, the integral equation (4.64) can be written in discrete form as follows

$$-\frac{1}{2}\varphi_{0n,i} = \sum_{j \in Q} (g_{ij} \varphi_{0nx_0,j}) \quad \forall i \in Q, \quad (4.67)$$

where  $Q$  is the set of panels belonging to the segment  $[-b/H, b/H]$ , and  $\varphi_{0n,i}$  and  $\varphi_{0nx_0,i}$  denote the velocity potential and its derivative on panel  $i$ , and

$$g_{ij} = \int_{a_j-l_j}^{a_j+l_j} G(\mathbf{x}_i, \mathbf{x}_{0j}) dy_{0j},$$

where  $a_j$  is the middle point of the  $j$ -th panel and  $l_j$  is the distance between the  $j$ -th panel's middle point and its endpoints. Therefore,

$$g_{ij} = \frac{1}{\pi} \int_{a_j-l_j}^{a_j+l_j} K_0(\sigma_n \sqrt{x_i^2 + (y_i - y_{0j})^2}) dy_{0j}. \quad (4.68)$$

The velocity potential values along  $[-b/H, b/H]$  are known to be a constant by (4.30). If we compute  $g_{ij}$  in each panel, and replace them together with the velocity potentials in (4.67), will give us the horizontal velocities in each panel of  $[-b/H, b/H]$ .

For  $i \neq j$  and  $x_i = 0$ , equation (4.68) represents no problem and can be calculated by numerical methods, here we use the Trapezoidal rule

$$g_{ij} = \frac{l_j}{\pi} \left( K_0(\sigma_n |y_i - a_j + l_j|) + K_0(\sigma_n |y_i - a_j - l_j|) \right).$$

For  $i = j$  and  $x_i = 0$ , there is an integrable singularity at the mid point of the panel. We use the method "subtraction of singularity" to evaluate the integral and we use the limiting form of  $K_0(z)$  for small arguments (A.5)

$$K_0(z) \sim -\ln(z), \quad (4.69)$$

therefore  $g_{ij}$  can be written as

$$g_{ij} = \frac{1}{\pi} \int_{a_j-l_j}^{a_j+l_j} K_0((\sigma_n|y_i - y_{0j}|) + \ln(\sigma_n|y_i - y_{0j}|)) dy_{0j} - \frac{1}{\pi} \int_{a_j-l_j}^{a_j+l_j} \ln(\sigma_n|y_i - y_{0j}|) dy_{0j},$$

or

$$g_{ij} = \frac{1}{\pi} \int_{a_j-l_j}^{a_j+l_j} f_3(x_i, y_i, y_{0j}) dy_{0j} - \frac{1}{\pi} \int_{a_j-l_j}^{a_j+l_j} \ln(\sigma_n|y_i - y_{0j}|) dy_{0j}, \quad (4.70)$$

where

$$f_3(y_i, y_{0j}) = \begin{cases} 0 & y_i = y_{0j} \\ K_0(\sigma_n|y_i - y_{0j}|) + \ln(\sigma_n|y_i - y_{0j}|) & \text{otherwise.} \end{cases}$$

When  $y_i = y_{0j}$ , because of (4.69),  $f_3(y_i, y_{0j}) = 0$ , otherwise, when  $y_i \neq y_{0j}$ ,  $f_3(y_i, y_{0j})$  has to be calculated by numerical methods. Therefore, we split the first integral in (4.70) as following

$$\begin{aligned} \frac{1}{\pi} \int_{a_j-l_j}^{a_j+l_j} f_3(y_i, y_{0j}) dy_{0j} &= \frac{1}{\pi} \int_{a_j-l_j}^{a_j-\epsilon} K_0((\sigma_n|y_i - y_{0j}|) + \ln(\sigma_n|y_i - y_{0j}|)) dy_{0j} \\ &+ \frac{1}{\pi} \int_{a_j-\epsilon}^{a_j+\epsilon} K_0((\sigma_n|y_i - y_{0j}|) + \ln(\sigma_n|y_i - y_{0j}|)) dy_{0j} \\ &+ \frac{1}{\pi} \int_{a_j+\epsilon}^{a_j+l_j} K_0((\sigma_n|y_i - y_{0j}|) + \ln(\sigma_n|y_i - y_{0j}|)) dy_{0j}. \end{aligned} \quad (4.71)$$

As  $\epsilon \rightarrow 0$ , the second integral on the right of (4.71) is zero. This implies that (4.71) is regular. By applying the Trapezoidal rule

$$\frac{1}{\pi} \int_{a_j-l_j}^{a_j+l_j} f_3(y_i, y_{0j}) dy_{0j} = \frac{l_j - \epsilon}{\pi} (K_0(\sigma_n l_j) + \ln(\sigma_n l_j) + K_0(\sigma_n \epsilon) + \ln(\sigma_n \epsilon)),$$

which for  $\epsilon \rightarrow 0$  gives

$$\frac{1}{\pi} \int_{a_j-l_j}^{a_j+l_j} f_3(y_i, y_{0j}) dy_{0j} = \frac{l_j}{\pi} (K_0(\sigma_n l_j) + \ln(\sigma_n l_j)).$$

Using integration by parts, we can calculate analytically the second integral in (4.70)

$$-\frac{1}{\pi} \int_{a_j-l_j}^{a_j+l_j} \ln(\sigma_n |y_i - y_{0j}|) dy_{0j} = \frac{-2l_j}{\pi} (\ln(\sigma_n l_j) - 1).$$

To conclude

$$g_{ij} = \begin{cases} \frac{l_j}{\pi} (K_0(\sigma_n l_j) + \ln(\sigma_n l_j) - 2(\ln(\sigma_n l_j) - 1)) & i = j \\ \frac{l_j}{\pi} (K_0(\sigma_n |y_i - a_j + l_j|) + K_0(\sigma_n |y_i - a_j - l_j|)) & \text{otherwise.} \end{cases}$$

Now that we have the  $g_{ij}$  values, and  $\varphi_{0n}$  values from (4.30), replacing them in (4.67) yields

$$\frac{(-1)^n}{\sigma_n^2} = \sum_{j \in Q} (g_{ij} \varphi_{0nx_0,j}) \quad \forall i \in Q, \quad (4.72)$$

where  $n = 0, \dots, N$ . The solution of (4.72) gives the discrete values of  $\varphi_{0nx_0,j}$  in each  $j$  panel of  $[-b/H, b/H]$ .

The derivative of (4.28) with respect to  $x$  and truncation of the sum at  $n = N$ , for each  $j$  panel gives

$$\varphi_{0x,j}(0, y, z, t) = t \sum_{n=0}^N \varphi_{0nx,j}(0, y) \sin(\sigma_n z). \quad (4.73)$$

Replacing  $\varphi_{0nx,j}$  values in (4.73), provides the discrete velocities  $\varphi_{0x,j}(0, y, z, t)$  at each  $j$  panel for a fixed  $z$  from  $-1 < z \leq 0$ .

Before going to the numerical results, it is important to explain how the discretizations of  $y$  and  $z$  are done. The procedure follows the idea in Yilmaz et al. (2013a), that is, using a geometrical series to discretize the length of each panel. Two parameters are involved:  $a_m$ -the size of the smallest panel, and  $r$ -the growth factor. There are three critical regions: the first one  $x = 0, y = -b/H, -1 < z \leq 0$ , the second one  $x = 0, y = b/H, -1 < z \leq 0$  and the third one  $x = 0, -b/H \leq y \leq b/H, z = -1$ , therefore a denser discretization is required near them. The line  $-b/H \leq y \leq b/H$  is divided into



two equal segments,  $[-b/H, 0]$  and  $[0, b/H]$ , which are discretized separately. The smallest panel  $a_m$  is located near  $-b/H$  and  $b/H$  and the panels increase in size each time by multiplying with  $r$  as the panels approach  $y = 0$ . Similarly,  $-1 < z \leq 0$  is discretized by placing the smallest panel  $a_m$  near  $-1$  and increase the size of the panels by multiplication with  $r$  as they go near  $z = 0$ , see Fig. 4.5. Here the smallest panel size and the growth factor are chosen to be same to the ones in Yilmaz et al. (2013a), i.e.,  $a_m = 0.00001$  and  $r = 1.03$ .

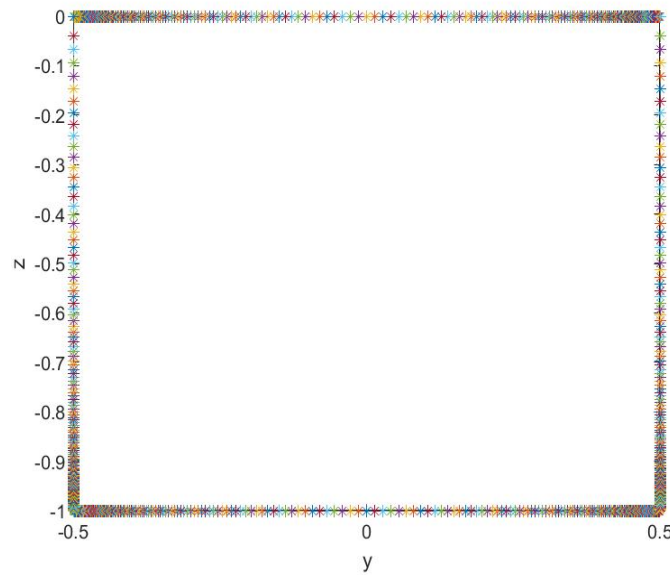


Figure 4.5. Discretization of the rectangular section

### 4.3. Numerical results

The numerical results of the boundary element method are provided in this section. We are interested in the horizontal velocities and the shape of the rectangular free surface. On this surface, along  $y = b/H$ ,  $y = -b/H$  and  $z = -1$ , the velocities perpendicular to the gate,  $\varphi_{0,x}$ , are expected to be singular, therefore a more careful discretization is needed near these lines. When discretizing  $[-b/H, b/H]$ , we start from the endpoints  $y = -b/H$  and  $y = b/H$ , by placing the smallest panel  $a_m$  close to them, and by increasing the length of each consecutive panel by a factor  $r$  as we approach  $y = 0$ . The length  $b/H$  is

discretized as

$$a_m + a_m r + \cdots + a_m r^{q-1} + \left( b/H - a_m \frac{1 - r^q}{1 - r} \right).$$

Therefore, the total number of panels in  $[-b/H, 0]$  is  $q + 1$ , where the length of the last panel placed near  $y = 0$  is  $b/H - a_m \frac{1 - r^q}{1 - r}$ . Similarly, the total number of panels in  $[0, b/H]$  is  $q + 1$ . If we combine the last two panels near  $y = 0$  into one segment  $[-b/H + a_m \frac{1 - r^q}{1 - r}, b/H - a_m \frac{1 - r^q}{1 - r}]$ , the total number of panels in  $Q$  becomes  $2q + 1$ , where

$$q = \lfloor \frac{\log(1 + b/H(r - 1)/a_m)}{\log r} \rfloor,$$

and  $\lfloor \cdot \rfloor$  is the floor function. Assuming  $b/H = 1/2$ , the growth factor  $r = 1.03$  and the smallest panel size  $a_m = 10^{-5}$ , we find  $q = 247$  and the total number of panels in  $[-1/2, 1/2]$  to be 495.

When discretizing  $[-1, 0]$ , the smallest panel  $a_m$  is placed near  $z = -1$  and the following panels grow with a factor  $r$ , as below

$$a_m + a_m r + \cdots + a_m r^{s-1} + \left( 1 - a_m \frac{1 - r^s}{1 - r} \right),$$

where  $1 - a_m \frac{1 - r^s}{1 - r}$  is the last panels length. Therefore, the total number of panels in  $[-1, 0]$  is  $s + 1$ , where

$$s = \lfloor \frac{\log(1 + (r - 1)/a_m)}{\log r} \rfloor = 270.$$

We study the horizontal velocities  $\varphi_{0,x,j}(0, y, z, t)$  of the rectangular free surface in two ways, first one, along constant  $z$  and second one along constant  $y$ .

Figure 4.6 shows the horizontal velocities  $\varphi_{0,x,j}(0, y, z, t)$  for  $j \in Q$ , and fixed  $z = -1, -0.9, -0.5, -0.1, 0$ . The horizontal velocities tend to minus infinity as  $y$  approaches  $b/H$  and  $-b/H$ . These figures show the presence of singularities along  $y = -b/H$  and  $y = b/H$ . From the calculations, we notice that, the horizontal velocities are symmetric with respect to  $y = 0$ .

The horizontal velocities  $\varphi_{0,x,j}(0, y, z, t)$  for the vertical lines at the rectangular section, where  $j \in S$ , for  $y = \pm 0.499, \pm 0.498, \pm 0.4, \pm 0.3, 0$ , where  $S$  is the set of panels of  $[-1, 0]$ , are represented in Fig. 4.7. Note that as  $z \rightarrow -1$ , the horizontal velocities of the rectangular free surface increase, indicating the singularities there.

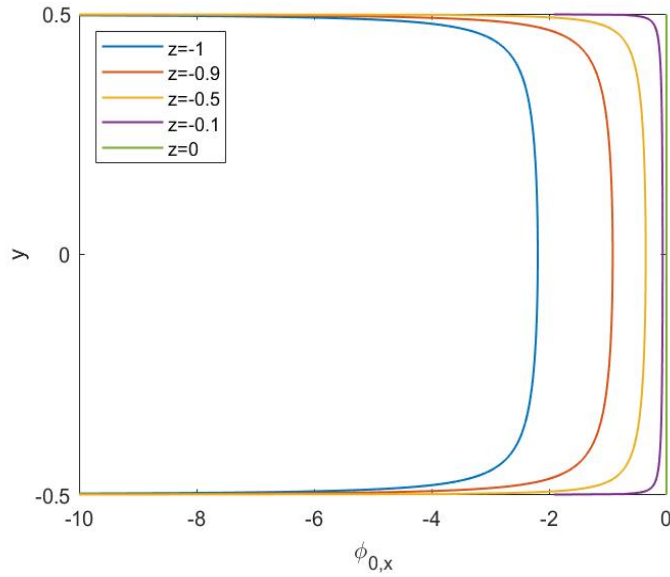


Figure 4.6. Horizontal velocities for  $z = -1, -0.9, -0.5, -0.1, 0$

The rectangular free surface shape is derived from (4.23). Due to the collapse, this rectangular flat surface, will become a 3-D shape. A grid is formed in the rectangular section by taking the horizontal and vertical lines. The curves along  $z$  for some fixed  $y \in Q$  and the curves along  $y$  for some fixed  $z$  in  $S$  are shown in Fig. 4.8 in order to give an idea about the 3-D form.

The shape of the special case when  $y = 0$  and  $z \in S$  is similar to the 2-D dam break problem by Korobkin and Yilmaz (2009), see Fig. 4.9.

From the shape of the rectangular free surface (Fig. 4.8) we can conclude that the singularity at  $y = \pm b/H$  is stronger than the one at  $z = -1$ . Using our experience from the corresponding two dimensional analysis (Korobkin and Yilmaz (2009) and Yilmaz et al. (2013a)) and Fig. 4.9, the singularity at the bottom,  $z = -1$ , is expected to be logarithmic. From the literature on water impact problems (Korobkin and Pukhnachov (1988) and Iafrati and Korobkin (2004)), the singularity at the sides of the gate,  $y = \pm b/H$ , is expected to be a power singularity. In that respect, as far as the singularity analysis is concerned, the problem is closer to water impact problems than to dam break problems. Korobkin and Pukhnachov (1988) and Iafrati and Korobkin (2004) claim square root singularity of the flow velocity at the intersection of the body with the liquid free surface.

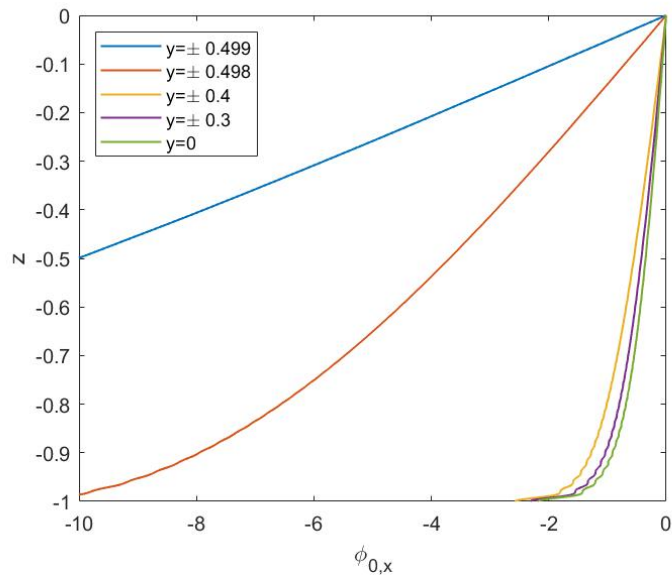


Figure 4.7. Horizontal velocities for  $y = \pm 0.499, \pm 0.498, \pm 0.4, \pm 0.3, 0$

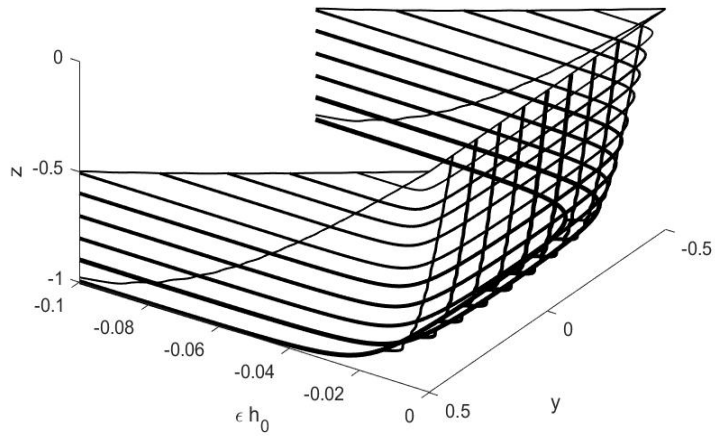


Figure 4.8. 3-D view of the vertical free surface at time  $t = 1$ ,  $\epsilon = 0.01$ , where on the vertical lines  $y = \pm 0.499, \pm 0.498, \pm 0.4, \pm 0.3, \pm 0.2, \pm 0.1, 0$ ,  $z \in S$ , and on the horizontal lines  $y \in Q$ ,  $z = -1, -0.9, -0.8, -0.7, -0.6, -0.5, -0.4, -0.3, -0.2, -0.1, 0$

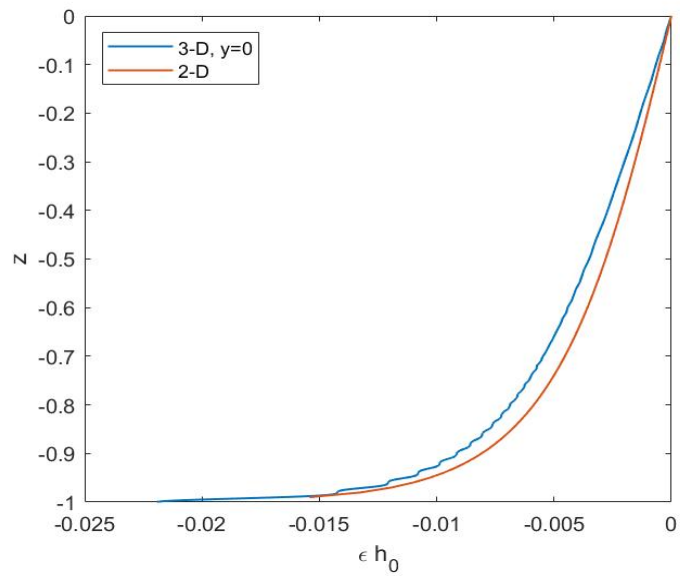


Figure 4.9. Vertical free surface at time  $t = 1$ ,  $\epsilon = 0.01$  for 3-D at  $y=0$  compared to 2-D

## CHAPTER 5

### CONCLUSIONS

In this thesis three 3-D problems on gravity-driven flow caused by the collapse of some cavity which is surrounded by an incompressible and inviscid fluid have been investigated for small times. On the early stage the flow is considered to be potential. The velocity potential and the free surfaces are expanded in a power series in terms of a small parameter representing small times. The linear leading order problems of the initial stage were solved using the Fourier series method for the first two problems and the boundary element method for the third problem. Our attention is focused on the singularities of the velocities and the shapes of the free surfaces within the mathematical model derived for the leading order problems for the velocity potential.

Chapter 2 provides the formulation and solution of the first problem on the gravity-driven flow caused by the collapse of a vertical cylinder of circular cross sections extending from a rigid bottom up to the free surface of a surrounding liquid that is resting on the rigid bottom and extending to infinity radially. This is the case of a dry-bed problem, which is important to be studied, because of the mismatch of the conditions on the circle where the initially vertical free surface and the rigid bottom meet. We observed that the velocity field close to this circle is singular within the mathematical model considered. An analysis of the singularity of the radial velocity at the bottom circle shows that the singularity is logarithmic, corresponding to the result of the 2-D dam-break problem by Korobkin and Yilmaz (2009), who actually from their study on the inner solution find a jet formation propagating along the dry bed. We concluded analytically and at the same time numerically that, as the radius and the centre of cavity approach infinity actually this problem reduces to the 2-D problem in Korobkin and Yilmaz (2009). This result is important, because it implies that at the bottom circle a jet formation will happen just like in the 2-D problem, without the need of resolving the inner problem close to this circle. We show that the larger the radius, the smaller the 3-D effects. The 3-D effects are important when the radius of the cavity is small compared to the height of the cavity.

In Chapter 3, we presented the second problem, which is another version of the

first problem, with the difference that the top of the cylinder starts from the top free surface, but is shallower than the height of the surrounding fluid. The difference in the cylinder's height, although at first glance may seem like a small modification, actually makes it as a different type of dam-break problem, the wet-bed one. We see that the mismatch of the conditions happen at the intersection of the initially vertical free surface with the lower free surface, which is the bottom circle of the cavity. Singularity analysis near this circle shows that the flow velocity is power singular  $r^{-1/3}$ , coinciding with the results of Yilmaz et al. (2013a) for two liquids of same density. Another result shows that as the radius and the centre of cavity approach infinity, this 3-D problem reduces to the 2-D dam-break problem of two immiscible fluids with different heights in Yilmaz et al. (2013a). The non-linear analysis described in Yilmaz et al. (2013b), indicates the formation of a jet at the corner point of the 2-D problem, therefore it is concluded that similarly here there is a jet formation expected near the bottom circle. The 3-D effects are unimportant when the radius of the cavity increases. When the radius of the cavity is small compared to the height, the 3-D effects become important.

Finally, in Chapter 4, we formulated and solved the third problem on the gravity-driven flow resulting from the collapse of a rectangular section of a vertical plate with height  $H$  placed in front of a fluid. The plate extends to infinity along the  $y$ -axis and is located in front of a fluid with height  $H$  that rests on a rigid bottom and extends to infinity along  $y$ -axis and positive  $x$ -axis. Mismatch of the conditions are noticed along the line where the initially vertical free surface and the rigid bottom intersect. Solution by boundary element method reveals that close to this line and close to the lines where the initially vertical free surface with the rigid plate intersect, the horizontal velocities of the initially vertical free surface increase in the negative direction, indicating the presence of singularities there. The vertical free surface shape also deflects when approaching these lines. Based on the shape of the free surface and on the results of Korobkin and Yilmaz (2009), Yilmaz et al. (2013a) and Korobkin and Pukhnachov (1988), logarithmic singularity is predicted along the intersection of the vertical free surface with the rigid bottom and power singularity  $r^{-1/2}$  is expected at the lines where the initially vertical free surface meets the rigid plate. It is observed that the shape of the initially vertical free surface along the vertical axis is similar to the shape on the initially vertical free surface in Korobkin and Yilmaz (2009). The 3-D effects are important when the length of the

rectangle is small compared to its width, otherwise when the length is big, they become unimportant.



## REFERENCES

- Abramowitz, M. and I. A. Stegun (1972). *Handbook of mathematical functions with formulas, graphs, and mathematical tables* (10th ed.). Wiley.
- Acheson, D. J. (2005). *Elementary Fluid Dynamics*. Oxford University Press.
- Bell, S. W., R. C. Elliot, and M. H. Chaudhry (1992). Experimental results of two-dimensional dam-break flows. *Journal of Hydraulic Research* 30(2), 225–252.
- Benusiglio, A., D. Quere, and C. Clanet (2014, 07). Explosions at the water surface. *Journal of Fluid Mechanics* 752, 123–139.
- C. King, A. and D. Needham (1994, 06). The initial development of a jet caused by fluid, body and free-surface interaction. Part 1. A uniformly accelerating plate. *Journal of Fluid Mechanics* 578, 89 – 101.
- Fenner, R. (2014). *Boundary element methods for engineers: Part I: Potential problems* (first ed.). bookboon.com.
- Fraccarollo, L. and E. F. Toro (1995). Experimental and numerical assessment of the shallow water model for two-dimensional dam-break type problems. *Journal of Hydraulic Research* 33(6), 843–864.
- Glasheen, J. W. and T. A. McMahon (1996a, 03). A hydrodynamic model of locomotion in the basilisk lizard. *Nature* 380, 340–342.
- Glasheen, J. W. and T. A. McMahon (1996b, 08). Vertical water entry of disks at low froude numbers. *Physics of Fluids* 8(8), 2078–2083.
- Haberman, R. (2013). *Applied partial differential equations with Fourier series and boundary value problems*. Pearson Higher Ed.
- Hudde, H. and U. Letens (1985). Scattering matrix of a discontinuity with a nonrigid wall

- in a lossless circular duct. *The Journal of the Acoustical Society of America* 78.
- Iafrazi, A. and A. A. Korobkin (2004). Initial stage of flat plate impact onto liquid free surface. *Physics of Fluids* 16(7), 2214–2227.
- Janosi, I., D. Jan, G. Szabo, and T. Tel (2004, 08). Turbulent drag reduction in dam-break flows. *Experiments in Fluids* 37, 219–229.
- Korobkin, A. and O. Yilmaz (2009). The initial stage of dam-break flow. *Journal of Engineering Mathematics* 63(2-4), 293–308.
- Korobkin, A. A. and V. V. Pukhnachov (1988). Initial stage of water impact. *Annual Review of Fluid Mechanics* 20(1), 159–185.
- Lauber, G. and W. H. Hager (1998). Experiments to dambreak wave: Horizontal channel. *Journal of Hydraulic Research* 36(3), 291–307.
- Linton, C. M. (1998, 01). The Green’s function for the two-dimensional Helmholtz equation in periodic domains. *Journal of Engineering Mathematics* 33, 377–401.
- Morse, P. M. and H. Feshbach (1953). *Methods of theoretical physics* (first ed.). McGraw-Hill Book Company.
- Needham, D., P. Chamberlain, and J. Billingham (2008, 07). The initial development of a jet caused by fluid, body and free surface interaction. Part 3. An inclined accelerating plate. *The Quarterly Journal of Mechanics and Applied Mathematics* 61.
- Pohle, F. (1950). *The Lagrangian equations of hydrodynamics: solutions which are analytic functions of time. PhD dissertation*. New York University, USA.
- Renzi, E. and F. Dias (2012, 04). Resonant behaviour of an oscillating wave energy converter in a channel. *Journal of Fluid Mechanics* 701, 482.
- Renzi, E. and F. Dias (2013). Hydrodynamics of the oscillating wave surge converter in the open ocean. *European Journal of Mechanics - B/Fluids* 41, 1 – 10.

- Simon, M. J. and F. Ursell (1984). Uniqueness in linearized two-dimensional water-wave problems. *Journal of Fluid Mechanics* 148, 137 – 154.
- Singh, V. P. (1996). *Dam breach modeling technology*. Springer, Dordrecht.
- Stansby, P. K., A. Chegini, and T. C. D. Barnes (1998). The initial stages of dam-break flow. *Journal of Fluid Mechanics* 374, 407 – 424.
- Stoker, J. J. (1957). *Water waves*. Interscience Publishers Inc, New York.
- Truscott, T. T., B. P. Epps, and J. Belden (2014). Water entry of projectiles. *Annual Review of Fluid Mechanics* 46(1), 355–378.
- William George Penney, F. R. S. and C. K. Thornhill (1952). Part iii. the dispersion, under gravity, of a column of fluid supported on a rigid horizontal plane. *Philosophical Transactions of the Royal Society of London. Series A, Mathematical and Physical Sciences* 244(882), 285 – 311.
- Yilmaz, O., A. Korobkin, and A. Iafrati (2013a). The initial stage of dam-break flow of two immiscible fluids. Linear analysis of global flow. *Applied Ocean Research* 42, 60 – 69.
- Yilmaz, O., A. Korobkin, and A. Iafrati (2013b). The initial stage of dam-break flow of two immiscible fluids. Nonlinear analysis. *Unpublished notes*.

# APPENDIX A

## MODIFIED BESSEL FUNCTIONS $I$ AND $K$

### A.1. Definition and properties

The solutions to the modified Bessel differential equation

$$w^2 \frac{d^2 f}{dw^2} + w \frac{df}{dw} - (w^2 + m^2)f = 0$$

are denoted by  $I_m(w)$  and  $K_m(w)$  and are known as the modified Bessel functions.

$I_m(w)$  is called the modified Bessel function of order  $m$  of the first kind. It is defined to be well behaved at  $w = 0$

$$I_m(w) \sim \frac{1}{m!} \left(\frac{1}{2}w\right)^m,$$

and exponentially growing as  $w \rightarrow \infty$

$$I_m(w) \sim \sqrt{\frac{1}{2\pi w}} e^w \quad (\text{A.1})$$

from (7.9.43) and (7.9.44) in Haberman (2013).  $K_m(w)$  is called the modified Bessel function of order  $m$  of the second kind. It is defined to be singular at  $w = 0$

$$K_m(w) = \begin{cases} \ln w & m = 1 \\ \frac{1}{2}(m-1)! \left(\frac{1}{2}w\right)^{-m} & m \neq 1, \end{cases}$$

and decaying as  $w \rightarrow \infty$

$$K_m(w) \sim \sqrt{\frac{\pi}{2w}} e^{-w} \quad (\text{A.2})$$

from (7.9.42) and (7.9.41) in Haberman (2013).

## A.2. Asymptotic expansions for large arguments

When  $m$  is fixed,  $w$  is large and  $\mu = 4m^2$ ,

$$I_m(w) \sim \frac{e^w}{\sqrt{2\pi w}} \left[ 1 - \frac{\mu - 1}{8w} + \frac{(\mu - 1)(\mu - 9)}{2!(8w)^2} - \frac{(\mu - 1)(\mu - 9)(\mu - 25)}{3!(8w)^3} + \dots \right], \quad (\text{A.3})$$

$$K_m(w) \sim \sqrt{\frac{\pi}{2w}} e^{-w} \left[ 1 + \frac{\mu - 1}{8w} + \frac{(\mu - 1)(\mu - 9)}{2!(8w)^2} + \frac{(\mu - 1)(\mu - 9)(\mu - 25)}{3!(8w)^3} + \dots \right], \quad (\text{A.4})$$

from (9.7.1) and (9.7.2) in Abramowitz and Stegun (1972).

## A.3. Limiting forms for small arguments

For  $m$  fixed and  $z \rightarrow 0$ ,

$$K_0(z) \sim -\ln(z), \quad (\text{A.5})$$

$$K_m(z) \sim \frac{1}{2} \Gamma(m) \left( \frac{1}{2} z \right)^{-m} \quad (\text{A.6})$$

from (9.6.8) and (9.6.9) in Abramowitz and Stegun (1972).

## A.4. Differentiation with respect to $w$

$$\frac{\partial I_m(w)}{\partial w} = \frac{m}{w} I_m(w) + I_{m+1}(w) \quad (\text{A.7})$$

$$\frac{\partial K_m(w)}{\partial w} = \frac{m}{w} K_m(w) - K_{m+1}(w) \quad (\text{A.8})$$

## APPENDIX B

### DIRAC DELTA FUNCTION

The Dirac delta function  $\delta(x - x_i)$  is a concentrated source at  $x = x_i$  defined as follows

$$\delta(x, x_i) = \begin{cases} 0 & x \neq x_i \\ \infty & x = x_i. \end{cases}$$

The fundamental operator property of the one-dimensional Dirac delta function for any continuous function  $f(x)$  is

$$f(x) = \int_{-\infty}^{\infty} f(x_i)\delta(x - x_i)dx_i.$$

In the case of two-dimensional Dirac delta function  $\delta(\mathbf{x} - \mathbf{x}_0)$

$$f(\mathbf{x}_0) = \int_{-\infty}^{\infty} \int_{-\infty}^{\infty} f(\mathbf{x})\delta(\mathbf{x} - \mathbf{x}_0)dA, \quad (\text{B.1})$$

where  $f(\mathbf{x}) = f(x, y)$ .

Dirac delta function has unit area

$$\int_{-\infty}^{\infty} \delta(x - x_i) = 1$$

and is even

$$\delta(x - x_i) = \delta(x_i - x).$$

From (9.3.26), (9.3.27), (9.3.28), (9.3.29), (9.3.30) and (9.5.4) in Haberman (2013).

## APPENDIX C

### GREEN'S FUNCTION FOR THE HELMHOLTZ EQUATION

The Green's function for the Helmholtz equation

$$\nabla^2 \varphi_{0n} + k^2 \varphi_{0n} = 0,$$

for some boundary conditions on a closed surface, is the solution of the inhomogeneous Helmholtz equation

$$\nabla^2 G(\mathbf{x}, \mathbf{x}_0) + k^2 G(\mathbf{x}, \mathbf{x}_0) = -4\pi\delta(\mathbf{x} - \mathbf{x}_0),$$

with homogeneous bc. The solutions of the Helmholtz equation symmetric about  $R = 0$  are the solutions of the equation

$$\frac{1}{R} \frac{d}{dR} \left( R \frac{dG}{dR} \right) + k^2 G = 0. \quad (\text{C.1})$$

Under the transformation  $kR = \bar{R}$ , C.1 becomes the Bessel's differential equation of order zero

$$\bar{R}^2 \frac{\partial^2 G}{\partial \bar{R}^2} + \bar{R} \frac{\partial G}{\partial \bar{R}} + \bar{R}^2 G = 0,$$

whose general solution is

$$G = c_1 J_0(\bar{R}) + c_2 Y_0(\bar{R}),$$

where  $J_0(\bar{R})$  is the Bessel's function of the first kind of order 0, and  $Y_0(\bar{R})$  is the Bessel's function of the second kind of order 0. We are looking for solutions that are singular at  $\bar{R} = 0$ , therefore  $c_1 = 0$  and

$$G = c_2 Y_0(\bar{R}).$$

From equation (9.1.9) in Abramowitz and Stegun (1972), the limiting form for small arguments of the Bessel's function of the second kind of order zero is

$$Y_0(\bar{R}) \sim -iH_0^{(1)}(\bar{R}),$$

where  $H_0^{(1)}(\bar{R})$  is the Hankel's function of the first kind and  $i$  the imaginary unit. Equation (7.2.18) in Morse and Feshbach (1953) shows that the required Green's function is

$$G = i\pi H_0^{(1)}(kR). \tag{C.2}$$



# VITA

**Date and Place of Birth:** 06.03.1990, Elbasan - Albania

## EDUCATION

### **2015 - present Doctor of Philosophy in Mathematics**

Graduate School of Engineering and Sciences, Izmir Institute of Technology,  
Izmir - Turkey

Thesis Title: Asymptotic behaviour of gravity driven free surface flows resulting from  
cavity collapse

Supervisor: Prof. Dr. Oğuz Yılmaz

### **2012 - 2014 Master of Science in Mathematics**

Department of Mathematics and its Applications, Central European University,  
Budapest - Hungary

Thesis Title: On semigroups of linear operators

Supervisor: Prof. Dr. András Bátkai

### **2008 - 2011 Bachelor of Mathematics**

Department of Mathematics, Faculty of Natural Sciences, University of Tirana,  
Tirana - Albania

## PROFESSIONAL EXPERIENCE

### **2014 - present Research and Teaching Assistant**

Department of Mathematics, Faculty of Natural Sciences, University of Elbasan,  
Elbasan - Albania

## PUBLICATIONS